Bacterial Cellulose Nanocomposites with Lignin:

Fabrication and Characterization of Structure, Mechanical & Thermal Properties

Xinsui Luo

A thesis

submitted in partial fulfillment of the

requirements for the degree of

Master of Science in Materials Science and Engineering

University of Washington

2021

Committee:

Eleftheria Roumeli

Anthony Dichiara

Program Authorized to Offer Degree:

Materials Science & Engineering

University of Washington

Abstract

Bacterial Cellulose Nanocomposites with Lignin:

Fabrication and Characterization of Structure, Mechanical & Thermal Properties

Xinsui Luo (Esther Law)

Chair of the Supervisory Committee:

Prof. Eleftheria Roumeli

Department of Materials Science & Engineering

From 1950 to 2018, the production of synthetic plastics has grown dramatically from 1.5 million tons per year to 360 million tons per year [1]. The unsustainable production of synthetic plastics have not only introduced massive waste in the ocean, released greenhouse gases but also pose potential health threat to all life forms. Therefore, there is a significant need to produce sustainable polymers, from renewable recourses, that are either recyclable or biodegradable. Cellulose, the world's most abundant biopolymer is synthesized from plants, algae as well as some bacteria, and because of its exceptional properties, such as being bio-degradable, easily functionalizable, and having remarkable mechanical properties which are comparable to Kevlar and carbon fiber [2,3], it has received the significant attention during the past decades. Among many types of cellulose, bacterial cellulose (BC) fibers come in as a matrix-free form, and do not require purification process as complicated as wood-extracted cellulose. BC in the form of pure nanocellulose microfiber has been reported giving rise to materials with remarkable Young's modulus (~66GPa [2]), strength (~1GPa [2]), and toughness (16.9 MJ/m [2]) due to its high fiber aspect ratio, high crystallinity, and massive hydrogen bonding network [4,5]. However, BC-based materials are extremely hydrophilic due to the presence of their surface hydroxyl groups, and due to their high rigidity, they are also brittle. In natural wood, lignin, formed by phenolic monomers, serves as a binder, together with other polymers, for cellulose, providing rigidity to the plant cells wall, supporting water transport, adding hydrophobic characteristic, and protecting wood against microorganisms [3,6]. Recent literature shows that introducing lignin in wood-extracted cellulose fibers can create nanocomposite papers with improved mechanical properties, thermal stability and hydrophobicity compared to conventional cellulose paper [6].

In this work, we fabricate a series of BC/lignin nanocomposites through a design of experiments method which allows systematic investigation of processing conditions. In particular, we study the effects of hot pressing time (10-30 minutes), temperature (120-160 °C), and pressure (5-15 MPa) in the structure and mechanical properties of the BC/lignin nanocomposites, as well as in the control BC. We also examine the effects of lignin as a binder in single-layer and multi-layered BC/lignin configurations. Our characterization methods include scanning electron microscopy, thermogravimetric analysis, X-ray diffraction, tensile testing, contact angle analysis, and Fourier-transform infrared spectroscopy. We find that processing conditions affect both the single-layer BC and BC/lignin nanocomposites. In the single-layer BC, the introduction of lignin improves the elongation to break, at the expense of Young's modulus and strength. In the multi-layered BC, the Young's modulus and strength increase in the nanocomposites compared with the pure BC, demonstrating the efficiency of lignin as a binder for multi-layered cellulose composites. Moreover, we find both processing and introduction of lignin can improve the hydrophobicity of BC.

I. Table of Contents

II. List of Figures

III. List of Tables

IV. Acknowledgments

First, I would like to give my deepest gratitude and uncountable thanks to my academic advisor, Prof. Eleftheria Roumeli, for being a very helpful support and passionate guider during my entire master journey. My sincere thanks for Prof. Anthony Dichiara for giving me many useful advice and inspiration to help me further polish my research. I'm profoundly grateful to Dr. Andrew Jimenez, Mallory Parker, and Jeremy Fredricks who have been giving invaluable support in this project. My research would have been impossible without them.

Special thanks to Dr. Bichlien Nguyen and Dr. Karin Strauss from Microsoft Research, for guiding this project along the way. Additional thanks to Microsoft Research, who provided funding to this project.

Lastly, I would like to thank Hareesh Iyer, Chelsea Ho, Jeffery Hsu, Marissa Nelsen and all the members from Prof. Roumeli's research group, for being very collaborative fellows and provide suggestions and help to my research. Final thanks to Amanda Inthavong who has kept great accompany and friendships for four years.

1. Introduction

1.1. Motivations

Synthetic plastic is defined as long chain manmade polymeric molecules derived from oil [7]. Plastic is everywhere. Nowadays, the production of synthetic plastic has growth from 1.5 million tons in 1950 to 373 million tons in 2019 [8]. In 2015, about 6300 million tons of plastic waste had been produced, among which only around 9% had been recycled, 12% was incinerated, and 79% was disposed in landfills or in nature [9]. The process of making synthetic plastic is not sustainable, not only because the source of making plastic is not regenerable, and because of the low-recycling rate, but also because the degradation of synthetic plastic can take up to 20 to 500 years [10]. The degradation has great impact on ecosystem, such as leakage to the oceans, greenhouse gas emissions and recent studies raise remarks related to impact to the human health [9,10]. Therefore, there's urgent need to produce more sustainable materials that combine the ability to be synthesized from renewable resources with biodegradability and desired performance. Sustainable polymers can be categorized into two types: natural polymers, and synthetic biobased polymers. Natural biobased polymers or biodegradable polymers are obtained from renewable resources such as algae, plants, or bacteria [11]. Natural polymers such as cellulose, lignin, hemicellulose, starch, protein, and modified biopolymers, have been widely used in bioplastics and composites [12]. Synthetic biobased polymers are derived from different types of biomass such as plant oils, fatty acids, furan, terpenes, rosin acids, and amino acids [12]. In 2020, the total production volume of biobased polymers was 4.2 million tons, which is only 1% of the total production volume of fossil based synthetic polymers [8], indicating a huge market and upgoing trend in biobased polymer industry.

1.2. Biomass-based materials

The most abundant biobased polymers are chitin, silk, and cellulose, which are the fundamental building blocks of many biomasses such as plants, microorganism, fungi or bacteria. The presence of inter- and intra- molecular hydrogen bonding in those biobased polymers enables strong interactions which vary significantly based on the based on the structure and molecular backbone.

Cellulose, the most abundant biopolymer, is a polysaccharide which is naturally generated by plants algae, bacteria, and some fungi (Figure 1). There exist four polymorphs of cellulose, I ($I_\alpha$and I_β), II, III and IV. In nature, only cellulose I and II are found, while III and IV can be transformed through physical or chemical processing through cellulose I and II [3]. Pure cellulose in single fiber form has remarkable mechanical properties. The mechanical properties are greatly depended on the size, crystallinity, and aspect ratio of the fiber. Table 1 has shown difference of Young's modulus of cellulose from various types of sources, measuring type, and processing method. A pure crystalline cellulose such as cellulose I_α and I_β can have elastic modulus over 100GPa [3]. Bacterial cellulose also has remarkable mechanical properties, which are higher than many plant-derived cellulose fibers, due to the higher aspect ratio and high crystallinity of bacteria cellulose fiber.

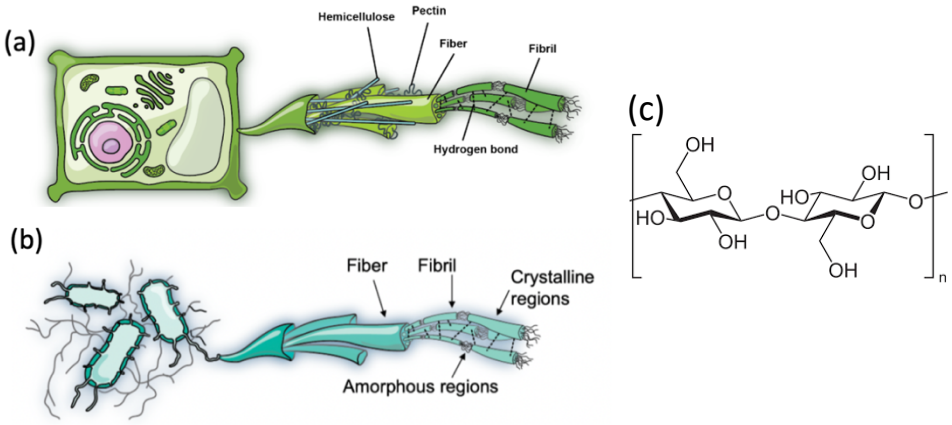

Figure 1. Biopolymer building blocks of plant cellulose (a) and bacterial cellulose (b). Chemical structure of cellulose polymer (c). Images (a) and (b) are adapted from [13].

Table 1.Young's modulus of different cellulose measured by different techniques [3].

Material	E_A (GPa)	E_T (GPa)	Technique
WF	14–27	—	Tensile
PF	5–45	—	Tensile, Raman
MCC	25 ± 4	—	Raman
MFC & NFC	N/A	—	
CNC			
plant	57, 105	—	Raman
wood	—	18–50	AFM indentation
t-CNC	143	—	Raman
Acid[a]	151 ± 29	—	AFM-3pt bend
TEMPO[a]	145 ± 31	—	AFM-3pt bend
	—	9 ± 3	AFM indentation
BC	78 ± 17	—	AFM-3pt bend
	114	—	Raman
Cellulose Iβ			
Experimental	120–138		XRD
	220 ± 50	15 ± 1	IXS
Modeling	110–173	—	
	137–168	10–50	
Cellulose Iα			
Modeling	128–155	5–8	
Cellulose II			
Experimental	9–90	—	Raman
Modeling	98–109	17–31	

1.2.1. Bacterial Cellulose

1.2.1.1 Bacterial cellulose structure

Bacterial cellulose (BC), can be synthesized through various bacterial species, including *Achromobacter, Alcaligenes, Aerobacter, Agrobacterium, Azotobacter, Gluconacetobacter, Pseudomonas, Rhizobium, Sarcina, Dickeya, and Rhodobacter* [14]. They can produce cellulose fibers through metabolic synthesis of sugar. These fibers would bundle up to form microfibrils and fibrillar ribbons, forming a pellicle matrix at the interface of liquid culture media and air. BC pellicles are hydrogels with hydrophilic network structures that can absorb from 20% to 1000 times their dry weight in water [3]. A porous structure is seen in the SEM image of bacterial cellulose in Figure 2 (b) and (c).

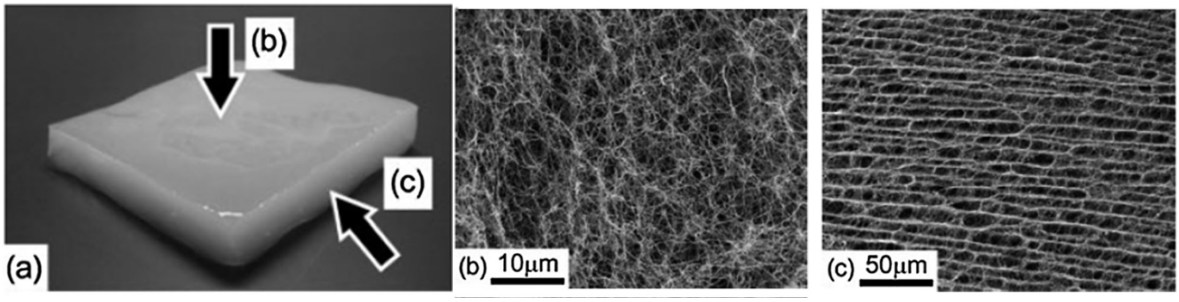

Figure 2. Images of BC pellicle. (a) optical image of BC wet pellicles with indications of image b and c directionality. Field-emission SEM image showing the (b) the in-plane BC network, and (c) the transverse structure. Adapted from [3].

1.2.1.2 Processing effects on bacterial cellulose

The structure and performance are highly dependent on the bacterial cellulose synthesis conditions (species, culture conditions), as well as on processing (pellicle cleaning, purification and dehydration processes) as well as further chemical or physical modifications [3]. Literature-reported effects of bacteria species [15], media [16], media pH [16], culture temperature [16] and agitation

[15] demonstrate changes on the structure and morphology (and subsequently mechanical properties) of the obtained cellulose fibers. For example, the BC fibrils produced from agitated cultures are more entangled as compared to the more elongated fibrils obtained from static culture [17]. The most commonly followed cleaning process, which requires the pellicle to be treated with low concentration of NaOH bath for a few hours, and then rinsed with water to remove the bacteria and neutralize the pH, which also influences the structure of the cleaned BC. Moreover, mechanical treatment can be employed to alter the structure of the pellicle, either by defibrillization of the pellicle to destroy the hydrogel matrix [18–20] or introduce stretching to achieve fiber alignment [21–23]. Regarding pellicle dehydration, water can be removed by simple evaporation or compression during evaporation, producing a densified film with density at about 1g/cm^3. Solvent exchange or freeze drying can also be used to remove water while minimize the BC microfibril consolidation during the evaporation [3]. The thickness of BC can be controlled by applying different drying methods. Finally, chemical or physical treatments can be applied to BC at any of the previously mentioned steps to achieve different morphologies and configurations, resulting in composites materials that have very different properties from the original BC [3].

1.2.1.3 Kombucha SCOBY bacterial cellulose culturing methods

Kombucha is a fermented tea beverage originated from North-Eastern China [24]. A Symbiotic Culture of Bacteria and Yeast (SCOBY) can be used as a starter in medium with tea extract and a sugar source, and upon culturing for 7-10 days, a BC pellicle can be obtained (Figure 3) [25]. A layer of cellulose is synthesized by the bacteria, and floats on the surface between the liquid media and air [26]. Since tea extract contains diverse vitamins and minerals, there's no need to introduce additional nitrogen sources to liquid media during the fermentation process, making

it an easier way to produce bacterial cellulose [26]. The yeast cells in SCOBY metabolize the sugar in the liquid media into glucose and fructose, which is subsequently used in the synthesis of cellulose biofilm by the bacteria [14]. This cellulose produced by bacteria is to provide attachment and protection to cells, preventing their exposure to the environment, protecting against ultraviolet radiation [27].

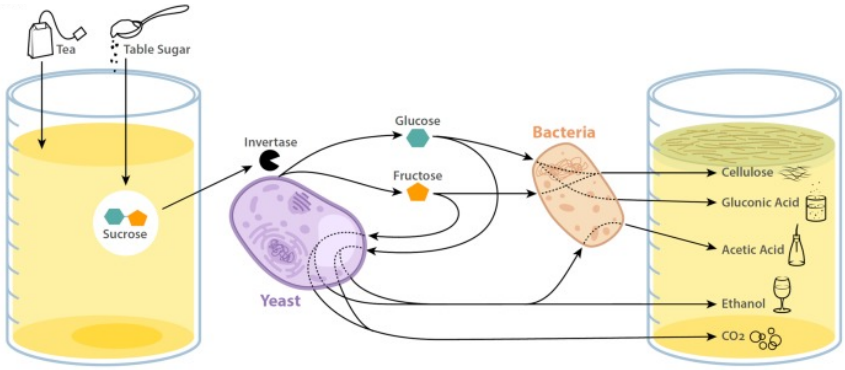

Figure 3. Kombucha SCOBY co-culturing by yeast cells and bacteria. Adapted from [28].

A commonly used method for preparing kombucha culture is by adding and stirring 0.5% of tea leaves and 5% sucrose in 1 L of boiling water. The tea leaves are filtered after 5 min of stirring and the temperature of the liquid media is cooled down to 20℃. 0.2% of kombucha tea and 3% of SCOBY pellicle is added to the media to lower the pH, which promotes the fermentation process and help avoiding other microbes growth. The container of mixture is then covered with a cloth to ensure aerobic respiration, and given 7-14 days to grow at 18℃ – 26℃ [29,30].

SCOBY consists of various microbial species, including *Gluconobacter, Acetobacter, Zygosaccharomyces, Saccharomyces, and Schizosaccharomyce.*[14]. Even though the type of microbes depends on many factors like the source, fermentation substrates, metabolites produced during the fermentation process [31], the majority type of bacteria used in SCOBY culture remains

unchanged [32], in which *Acetobacter xylinum* strain is the most commonly used strain in SCOBY cultures [33].

1.2.2. Bacterial-cellulose nanocomposites

Bacterial cellulose forms a 3-dimentional nano and micro fibrous porous network, and has remarkable and potentially tunable properties, including low density, high specific surface area, high absorption capacity, high strength, and high aspect ratio. BC is easy to process since it does not contain impurities such as lignin, hemicellulose, or pectin as in plant cellulose. Because of those attributes, it can potentially bind with different particles to form composite materials, such as silver particles, CNT, gelatin and so on, to expand wide range of properties and functionality [34].

The introduction of different types of particles or fillers, as well as using different mixing and post-processing methods, can be used to alter the mechanical properties of BC nanocomposites. For example, one study on silica/BC nanocomposites, shows the effects of introducing SiO_2 nanoparticles either directly in the BC culture media, or through soaking the harvested BC subsequently in a solution with SiO_2 nanoparticles [35]. The results show that the structure and mechanical properties of the composites present different trends in each type of composites. In the composites that the nanoparticles were introduced during the growth of BC, tensile strength decreases as the increase of silica content, while in the composites prepared by soaking, the silica content increases the tensile strength of the sample till 6% then decrease afterwards (Figure 6) [35].

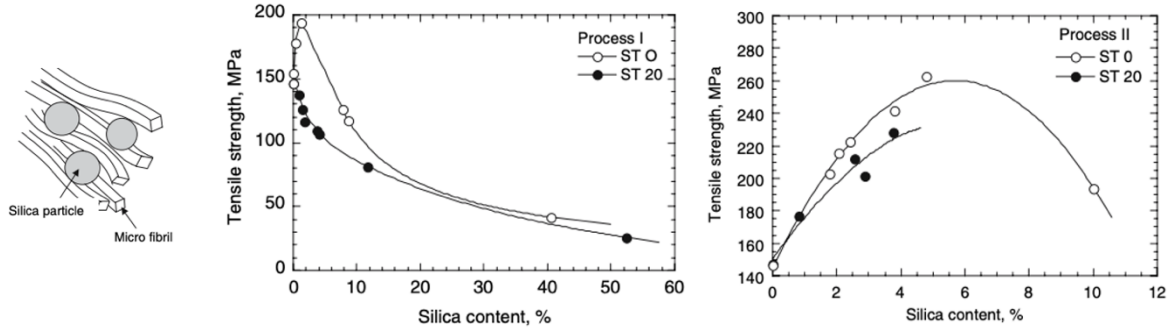

Figure 4. Mechanical properties changed with respect to silica content. (Process I, the silica was introduced during the culturing stage; Process I, the silica was penetrated by soaking and drying after the BC pellicle was formed. Adapted from [35].

Not only can BC be used as a matrix of the composites, but also it can be broken down into micro/nanofibrils and be used as a filler. In one study, BC was broken down to about 3μm particles by ultrasonication and casted into glycerol-starch bioplastic, with only 1% of BC in the bioplastic, the tensile strength reached up to 11.85 MPa, Young's modulus to 3.13 MPa, elongation at 4.11% and density of 0.42 g/cm^3 [36].

1.2.3. Lignin as a filler/matrix for nanocomposites

Lignin is a phenolic polymer mainly comprised of three constituent monomers or so called monolignol, p-hydroxyphenyl (4-hydroxyphenyl, P), guaiacyl (4-hydroxy-3-methoxyphenyl, G), and syringyl (4-hydroxy-3,5-dimethoxyphenyl, S), arranged in a hyperbranched topology with no regular repeating structure [37]. (Figure 5)

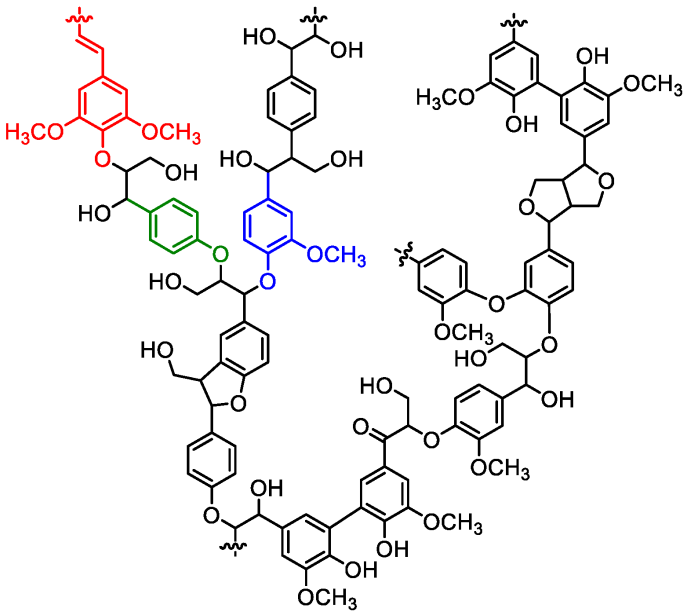

Figure 5. schematic representation of chemical structure of three precursors of lignin. (Major monolignol units are colored as sinapyl alcohol-red, guaiacyl alcohol-blue, p-coumaryl alcohol-green). Adapted from [38].

Lignin is one of the three major components in plant cell walls, and provides rigidity to the plants. Lignin aids internal transport of water, providing hydrophobicity to woods, protecting the plants against microorganisms. Kraft lignin is abundant since it is a by-product from pulping or paper making industry. Since cellulose by itself is very hydrophilic due to the presence of available hydrogen bonds, research on nanocomposites of micro/nano fibrillated cellulose with different types of kraft lignin has been conducted, showing an improvement of hydrophobicity after hot pressing in certain conditions (Figure 6). Hot-pressing allows lignin to soften, thus filling the voids between the fibrillar cellulose network [39].

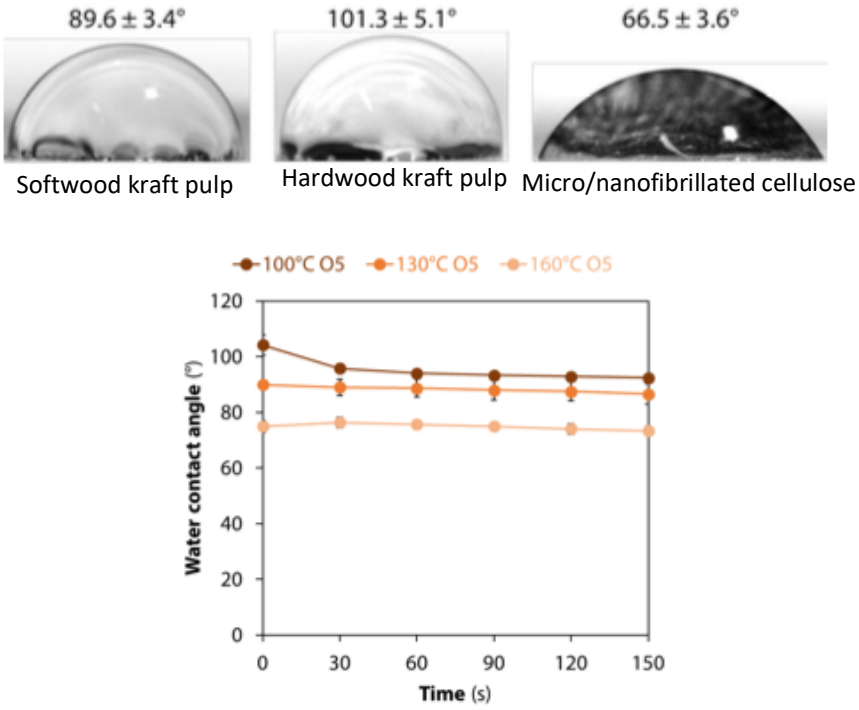

Figure 6. Contact angle of different lignin/cellulose composite, and the change of water contact angle over time with different processing conditions. Adapted from [39].

Recent literature shows that hot pressing can be used to create scalable high-performance lignin-cellulose papers, (Figure 7) [6]. The hot-pressed lignin-cellulose papers have a significantly improved performance, with mechanical properties 5 times higher in the composites (tensile strength = 200 MPa) than that in conventional cellulose paper (tensile strength = 40 MPa) [6]. The same report shows that the hydrophobic phenylpropane structure and the self-bonding of the lignin content under hot-pressing improved the water stability on the reinforced cellulose paper, which is similar to the role that lignin plays in natural wood.

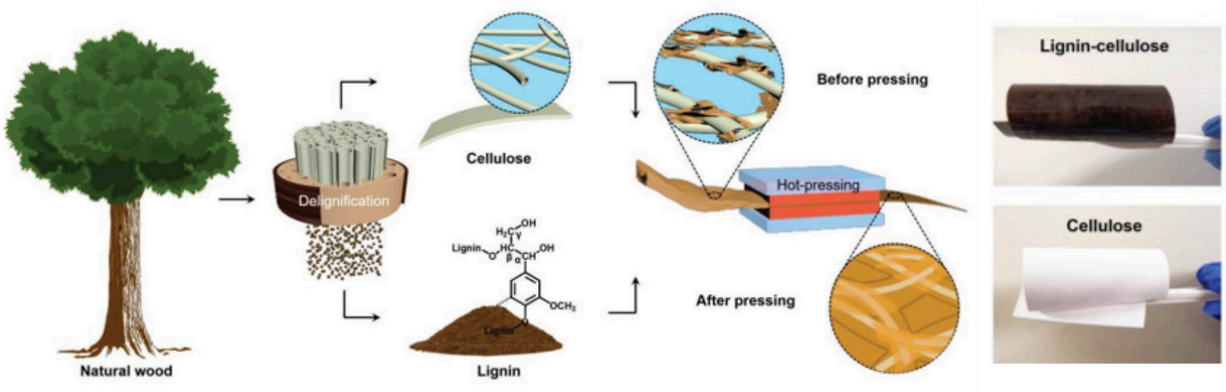

Figure 7. the production of lignin-cellulose nanocomposite. Adapted from [6].

1.3. Objectives

The goal of this work is to study the effects of lignin as a binder for BC nanocomposites and as a hydrophobicity modifier for BC. We target specifically to improve the extensibility of BC, the strength and stiffness in multi-layered composites and the hydrophobicity of the BC films.

We hypothesize that the introduction of lignin will improve the elongation to break in BC films as it can facilitate enhanced intermolecular interactions between neighboring cellulose fibrils. In addition, we propose that lignin can act as a binder in multi-layered BC structures, improving the Young's modulus and ultimate tensile strength of the composites by enhancing the load transfer between the cellulose fibers of the subsequent layers. Finally, the effectiveness of lignin in improving the water contact angle of BC will be tested.

In addition to the effects of lignin in the properties of BC, we seek to systematically evaluate the effects of processing conditions on tuning the structure and properties of pure BC and in BC/lignin nanocomposites.

2. Material and Methods

2.1. Materials

Tea bags, kombucha SCOBY starter, cane sugar and apple cider vinegar were commercially sourced. Lignin, alkali (CAS: 8068-05-1) and sodium hydroxide were purchased from Sigma Aldrich.

2.2. Bacterial Cellulose culture

2.2.1 Kombucha Bacterial Cellulose Culturing

Bacterial cellulose was cultured in a 5-gallon (16 x 8 x 10") tank using five major ingredients: black-tea tea bags, cane sugar, apple cider vinegar, and DI water. 2L of water was boiled and added into large beaker with 8 tea bags. The tea liquid medium was stirred using a magnetic stirrer mixer for 5 min at approximately 200 RPM. After 5min, tea bags were removed from the medium and then 800g of cane sugar was added. The mixture was stirred for 20 min at 200 RPM using a magnetic stirrer until all the cane sugar dissolved. Air cooling step to reduce temperature to around 40℃, and then added 800mL of apple cider vinegar and mix for 5min using a magnetic stirrer at approximately 200 RPM. The culture medium was poured into the tank, following the addition of another 2L of DI water. When temperature of the liquid media is about 30℃, about 60g of commercial SCOBY Kombucha Culture containing liquid and pellicle is introduced into the tank. Manual stirring for 5 min which can be achieved also with magnetic stirring for 5min at 200 RPM. Covered the tank with porous membrane to prevent contamination but allow air flow. Left the tank in room temperature for 15 days of culturing.

2.2.2 Kombucha Bacterial Cellulose Harvesting and Cleaning

Bacterial cellulose was harvested the as a sheet from the tank and immersed it into 1 liter of 1 mol/L sodium hydroxide solution. The solution was kept stirring at 90℃ for 1hr at 150 RPM. Air cooling the solution was followed by progressive dilution with deionized water till a neutral pH was achieved. The cellulose sheet was washed by rinsing in a beaker with deionized water for 2 times followed by 24 hours deionized water soaking and repeat the rinsing and soaking process for about 7 times or until the pH of the solution reaches 7 and the color of the pellicle turn from brown to white.

2.2.3. Lignin infiltration in bacterial cellulose

The wet and cleaned bacterial cellulose pellicle was submerged and stirred in 0.1g/mL of lignin solution at 150 RPM for 2 hours. The lignin solution was prepared by 40g of lignin and 400mL of deionized water stirring at 200 RPM till all the lignin dissolved.

2.2.4. Drying

Bacterial cellulose and lignin composite sheets were dried initially through vacuum filtration to remove excess lignin solution, followed by rolling using a pin in a layered configuration: water absorbent mat/steel mesh sheet/filter paper/BC-Lignin composite/filter paper/steel mesh sheet/ water absorbent mat (Figure 8). This stacked configuration was dried under a weight for 1-2 days until weight of the nanocomposite paper remained unchanged.

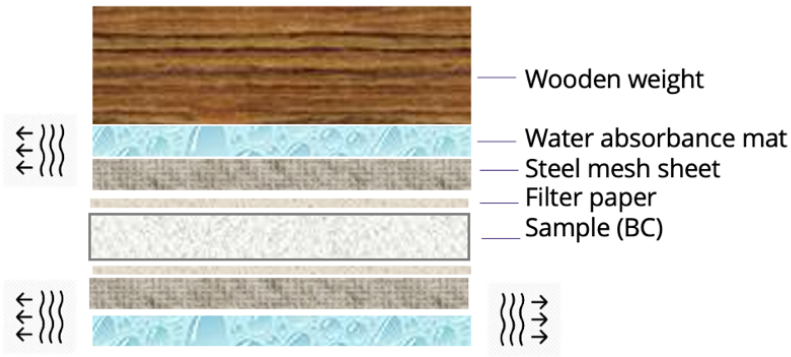

Figure 8. Schematics of bacterial cellulose air drying under a weight.

2.2.5. Post-treatment (Hot pressing conditions)

The air-dried nanocomposite papers were post-processed under hot press conditions. Firstly, by cold pressing at 40℃, 5Mpa for 5min and then three levels of each hot-pressing parameters of this study were: 1) pressing temperature: 120℃, 140℃, 160℃; 2) pressing pressure: 5 MPa, 10 MPa, 15 MPa; 3) pressing time: 10 min, 20 min, 30min. The conditions of hot pressing are listed in Table 2.

Table 2. Taguchi matrix of hot-pressing parameters of pure BC and BC/lignin nanocomposite.

Standard Run	Temperature (℃)	Pressure (MPa)	Time (min)
1	120	5	10
2	120	10	20
3	120	15	30
4	140	5	20
5	140	10	30
6	140	15	10
7	160	5	30
8	160	10	10
9	160	15	20

2.2.6. Effects of post-harvest processing

Three post-harvest drying processes were tested: freeze drying, air drying under a weight, and oven drying. Freeze dried was done by either freezer freeze dried for 24hr, or liquid nitrogen freeze dried for 2min until completely frozen. After frozen, samples were placed in freeze dryer (Freezone 2.5L, Labconco Coorporation, Kansas city, MO) at -50℃ for 24-48 hours to completed dryness with final equilibrium pressure at 0.02-0.03mBar.

Air dried under a weight was done by first pre-dried using a rolling pin process with water absorbent mat/steel mesh sheet/filter paper/BC-Lignin composite/filter paper/steel mesh sheet/ water absorbent mat configurations, followed by drying under a wooden weight with the same configurations. Oven drying was done by directly placing in a 60℃ oven (DVS602, Yamato Scientific, Tokyo, Japan) for 2 hours till the mass of the sample remained unchanged.

2.2. Fabrication of BC/lignin nanocomposites

Three fabrication methods for BC/lignin nanocomposite were tested to study the optimal method to introduce lignin into BC matrix. Processes included (a) lignin solution ultrasonication, (b) vacuum filtration, and (c) soaking upon stirring. Ultrasonication was done by submerging clean BC into prepared lignin solution and sonicate for 1 hour at room temperature followed by vacuum filtration to remove excess liquid. Vacuum filtration was done by placing BC on a filter paper in a funnel, then dropped in lignin solution while the vacuum pulling the solution through the BC. BC was flipped at least for three times during the process to ensure even distribution in both side of the sheet. Soaking was done by simply soaking BC in prepared lignin solution followed by gentle stirring using a magnetic stir bar at 150 RPM for 1 hour, and then remove the excess solution using vacuum filtration before the drying process.

2.3. Methods to Prepare Multi-layered Structures Pure BC and BC/lignin Papers

We also prepared and studied multi-layered structures of pure BC and BC/lignin nanocomposite. Both multi-layered papers were made by vacuum filtration to remove excess water at the first step. 1g/mL of lignin solution was introduced into BC matrix by hand spreading in between each layer and left in air for 5 min to absorb lignin. 4 layers of papers were stacked and air dried under a weight in water absorbent mat/steel mesh sheet/filter paper/BC-Lignin composite/filter paper/steel mesh sheet/ water absorbent mat configurations, until the mass of the paper remained unchanged. Each multi-layered paper was then cold pressed at 40℃, 5Mpa for 5min and hot pressed at 120℃, 5Mpa for 10min.

2.4. Characterization Methods and Analysis

2.4.1. SEM

The samples were coated with 5 nm of platinum in a Leica EM ACE600 sputter coater. SEM Imaging was conducted in a ThermoFisher Scientific Apreo variable-pressure SEM at an accelerating voltage of 10 kV. The images were acquired in a mixed BSE/SE (50%/50%) mode.

2.4.2. Mechanical properties

The tensile properties were measured using an Instron 3344, in accordance with ASTM D638 using a crosshead speed of 0.6% per seconds. Tensile test samples of about 600 – 800 μm thickness were prepared from hot pressing Taguchi matrix. Dumb-bell-shaped tensile test specimens were cut using a dog-bone-shape die press (central portion 0.5 mm thick, 12 mm gauge length). At least four measurements were conducted for each sample, and the results were averaged

to obtain a mean value. The values of Young's modulus, ultimate tensile strength at yield and at break point and elongation at break were calculated.

The stress (σ) and strain (ε) was calculated by the following equations:

$$\sigma(MPa) = \frac{F_{loading}(N)}{T_{thickness}(mm) * W_{width}(mm)}$$

$$\varepsilon\ (\%) = \frac{X_{displacement}(mm)}{L_{gauge}(mm)} * 100\%$$

Where F is the loading force of the Instron cell, X is the displacement of the grips, T, W, L corresponds to the thickness, width, and gauge length of the tensile test sample.

Showing from the Figure 9, the Young's modulus (E) was calculated by slope of the linear fitting at the first elastic region of the data using a python code. The ultimate tensile strength (UTS) was from the maximum tensile stress before breaking. The elongation to break was the strain at the breaking.

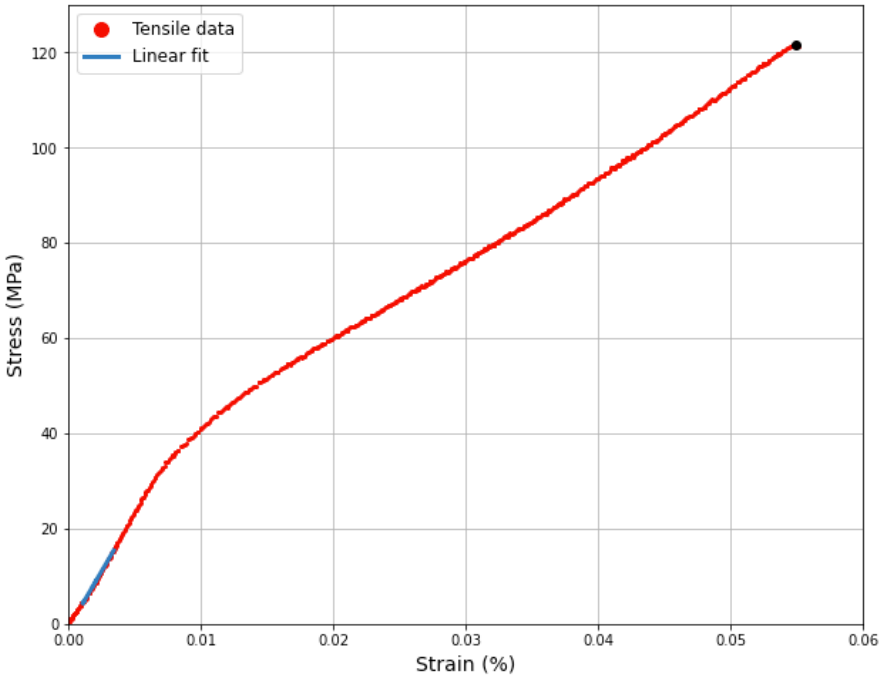

Figure 9. Tensile analysis example plot showing the linear region, ultimate tensile strength, and elongation to break.

2.4.3. Structural analysis (XRD & degree of crystallinity)

X-Ray diffraction (XRD) patterns were collected using PANalytical X'Pert Pro (Panalytical B.V., Holland) using an operating voltage at 40 kV, current at 40 mA, CuK_{α}, $\lambda = 0.1541$ nm. An angular range of $2\theta = 10 - 60°$ with a step size of 0.1° and a scanning speed of 0.008° s^{-1} was used for the measurements. XRD data was fitted with an exponential decay as baseline subtraction from the background substrate. The crystallinity (X_c) of the samples was calculated with the following equation [40]:

$$X_c = \frac{I_t - I_a}{I_t} * 100\%$$

I_t = intensity of crystalline peak at 22.7°

I_a= intensity of amorphous peak at 18°

2.4.4. Water uptake & contact angle measurements

Water uptake and thickness swelling test was modified from ASTM D1037 as mentioned in Sun et al. [41] 1 x 1 cm of air-dried sample was cut to measure the weight and dimensions. The thickness of the paper was measured using a caliper and the length and width of the sample were collected with ImageJ. Samples were submerged in 10mL of deionized water in a 50mL centrifuge tube. The mass and the size of the paper were measured at 2 hour and 24 hours after the submersion. Before each measurement, the samples were placed on a Kimwipe tissue and gently tabbed with Kimwipe tissue. Water retention ratio (%) was defined as the weight difference between wet and dried sample divided by the dried weight:

$$Water\ rentention\ ratio\ = \frac{W_{wet} - W_{dried}}{W_{dried}} * 100\%$$

Contact angle measurement were collected in DSA100 Drop Shape Analyzer from KRÜSS (Hamburg, Germany). Four 3μL sessile droplets were place on the sample at 20 ℃ in air environment for 15 seconds before taking the measurements of contact angle fitted by ellipse tangent at right and left side of the droplets.

2.4.5. Thermal properties (TGA)

TGA measurements were conducted in a D550 TGA from TA Instruments, (New Castle, DE). Samples were heated from room temperature to 1000℃ at a heating rate of 1℃/min in air flow at 40 mL/min.

2.4.6. Fourier transform infrared spectroscopy (FTIR)

FTIR spectra were collected with a ThermoNicolet iS10 spectrometer (Thermo Scientific, Waltham, MA, USA) equipped with an ATR crystal. The spectra were collected across the range of 400-4000 cm^{-1} with a resolution of 2 cm^{-1} and accumulated 64 scans for each spectrum.

3. Results & Discussion

3.1. Structure and Properties of Pure Single-layered BC Films

Kombucha bacterial cellulose was produced in lab after 15 days culturing. In Figure 10 we present the bacterial cellulose pellicle flowing on the liquid media in a tank before harvesting. On the right of the same figure, a harvested and cleaned bacterial cellulose pellicle after sodium hydroxide cleaning and water rinsing, is presented. That is the raw wet material used and referred to as BC in this project.

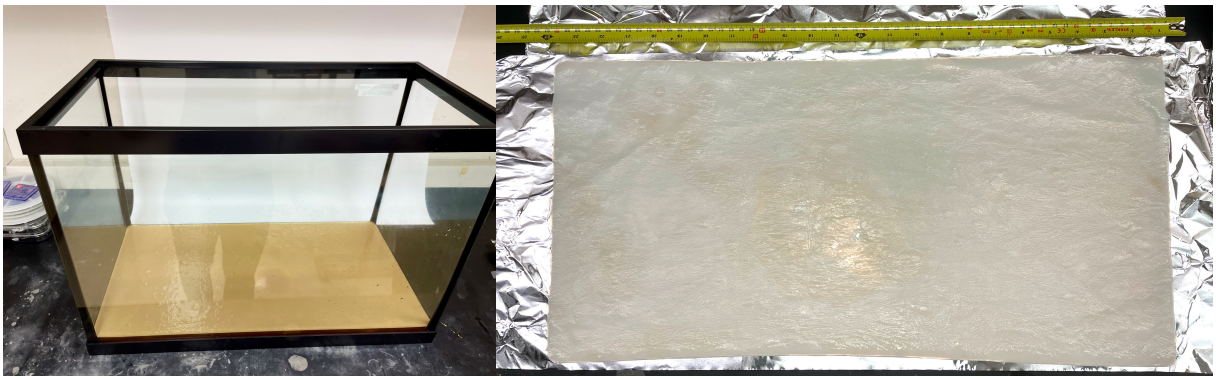

Figure 10. In lab Kombucha SCOBY co-culture after 15 days of culturing in a fish tank (left). Clean bacterial cellulose after washing with basic solutions and rinse with deionized water (Right).

After obtaining the raw wet bacterial cellulose, we studied different drying methods including oven drying, air drying, and freeze drying to determine the most efficient method to achieve flat, flexible single layer BC papers that have a smooth surface. As compared in Figure 11 and Figure 12, air drying under a weight was the optimal method to achieve a flat and smooth surface, while freeze dried BC were much more brittle, less flexible, and easy to facture.

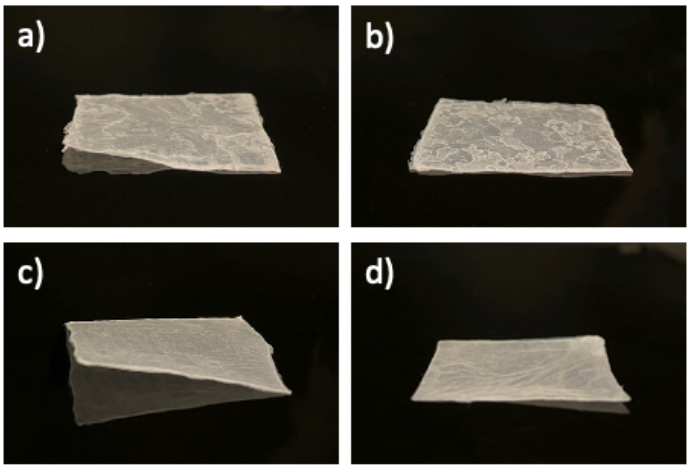

Figure 11. Drying method comparison between pure BC samples. a) Oven-drying at 60 ℃ for 2hr without weight on top of the sample; b) Oven-drying at 60 ℃ for 2hr with weight; c) Air-drying at room temperature without weight; d) Air-drying with weight.

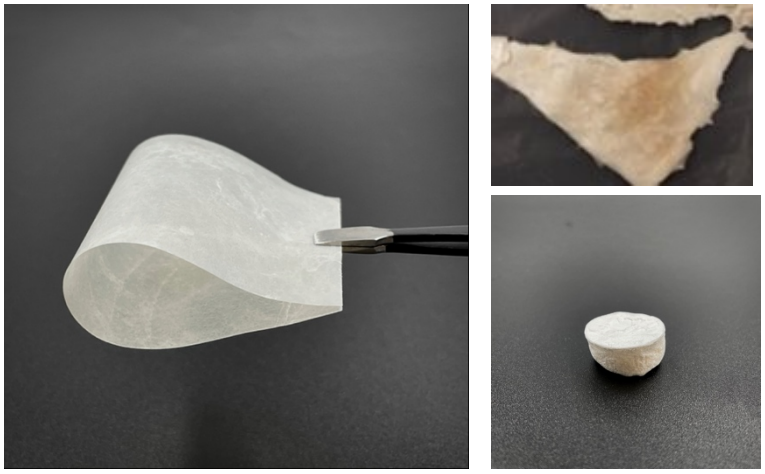

Figure 12. Bacterial cellulose after air-drying under a weight, showing the flexibility of sample (left). Liquid nitrogen freeze dried BC (bottom right). Freezer freeze dried BC (top right).

Tensile test results of pure single-layer air dried BC and freezer freeze dried BC are presented in Table 3. Liquid nitrogen freeze dried BC was too brittle to be cut into a dumb-bell shape specimen, and therefore only freezer freeze dried BC was tested for mechanical properties. Single-layer BC was nearly four times higher in Young's modulus, twice higher in ultimate tensile

strength and extensibility. As a result, air dried single layer BC was selected as the baseline properties for pure BC.

Table 3. Mechanical properties table for pure BC at air dried single layer BC form, and freezer freeze dried form.

Sample	Young's Modulus (GPa)	UTS (MPa)	Elongation to Break (%)
Single Layer BC	3.9	97.2	4.3
Freezer Freeze Dried	1.0	34.6	1.5

Water properties of pure BC was investigated through contact angle tests (surface properties, instant response) and a water uptake tests (bulk properties and long-term performance). In the contact angle testing, freeze dried BC immediately absorbed the water droplets (0º contact angle), indicating the presence of a completely wettable surface, as expected from the hydrophilic cellulose. Single-layer BC has much higher contact angle at around 44º indicating again a hydrophilic and wettable surface, but less so compared to the freeze-dried counterpart, possibly due to their vast difference in porosity (freeze-dried BC is more porous and less dense, thus cellulose fibers are interacting less, leaving more surface hydroxyl groups available to bind with water). In the water uptake test of air-dried single layer pure BC, the results showed a high water retention ratio after 2 hours and 24 hours of water submersion. (Figure 13)

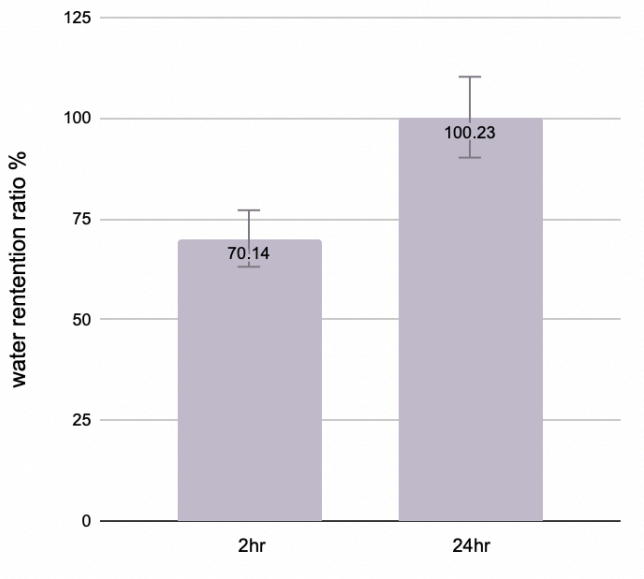

Figure 13. Water uptake test on single-layer pure BC after 2hr and 24hr.

3.2. Effects of thermo-mechanical processing of pure BC

Pure single-layer BC was processed through various conditions of hot pressing based on the Taguchi matrix. The effect of processing conditions was evaluated through mechanical properties, microstructure morphology, crystallinity and contact angle. The post processed pure BC sample was shown in Figure 14. Sample 1, 2 and 6 had the minimal discoloration, while sample 5, 7, 8 and 9 which were processed in either highest temperature or time were appeared brown after hot pressing.

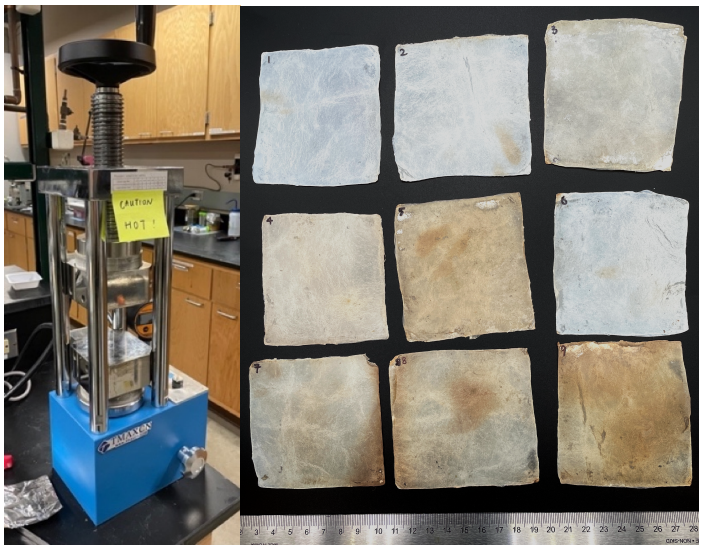

Figure 14. Hot press in the lab (left). Pure BC after hot pressing with various conditions. (right)

However, the morphologies characterized by SEM showed there was no difference in terms of microstructure at the tensile fractured surface across all the samples as seen in Figure 15. The microstructure revealed the anisotropic characteristic of single-layer BC. All hot-pressed samples were presented with a layer-by-layer morphology with BC nanofibrils dangling and interlocking each successive layer.

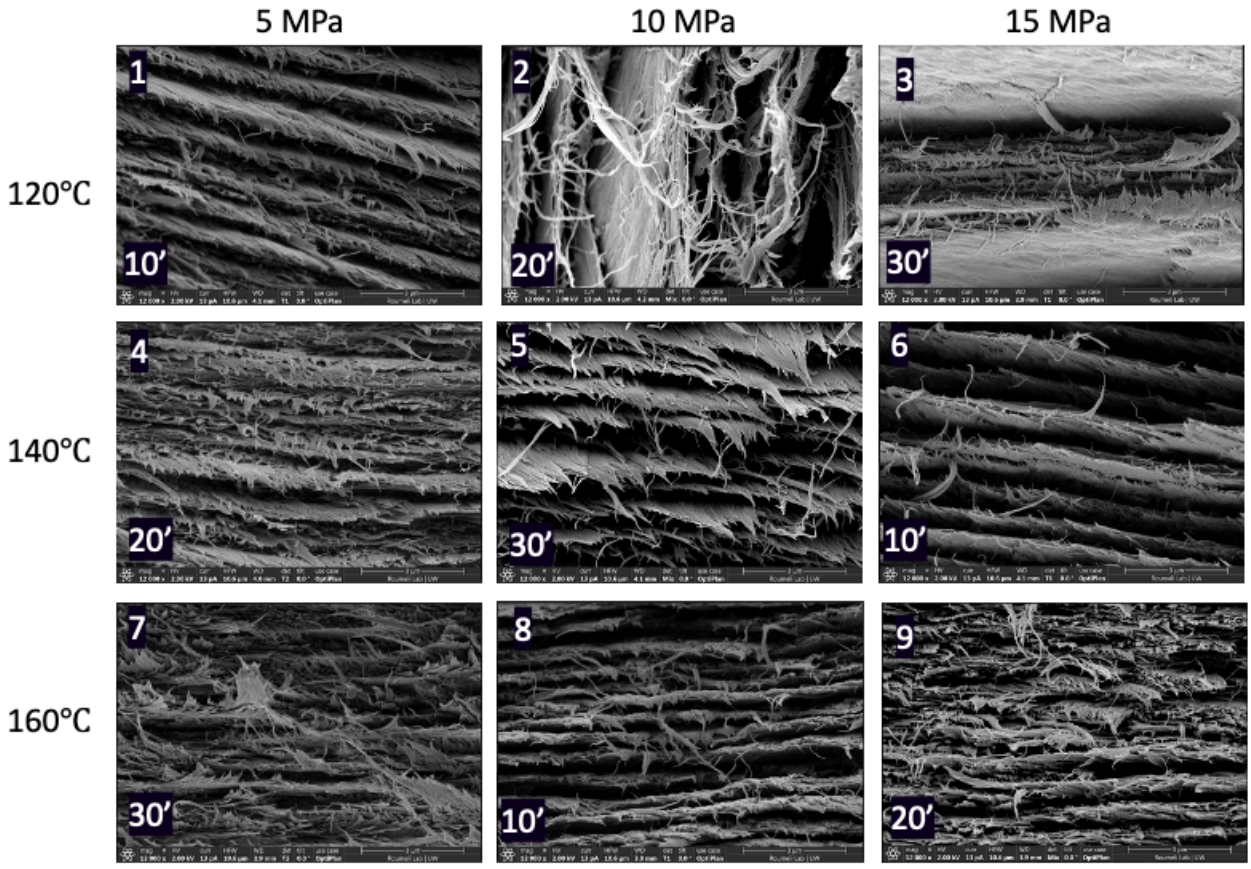

Figure 15. Pure BC sample processed with Taguchi matrix SEM images. Images were taken with failure of tension at the cross section.

We studied the mechanical properties of pure BC to find the conditions that gives the highest Young's modulus, ultimate tensile strength (UTS), and potentially elongation to break (EtB) as high as possible. We performed tensile testing and the results were shown in table 5. Three levels of Young's modulus, UTS, and EtB were selected by first and third quartile of the experimentally measured values (Table 4). The best mechanically performing samples were defined as those which combined maximum Young's modulus and UTS. The sample 6 processed at 140℃, 10 min, and 15 MPa as found with the best mechanical properties with both Young's modulus and UTS at L3, while sample 1 (120℃, 10 min, and 5 MPa) and sample 8 (160℃, 10 min,

and 10 MPa) was found to have the second-best mechanical properties with either Young's modulus or UTS at L3, and the other at L2.

Table 4. Assignment of mechanical results to three levels based on Quartile 1 and Quartile 3 on pure BC.

Level	Young's Modulus (GPa)	UTS (MPa)	Elongation to Break (%)
L1	<8.3	<143.4	<3
L2	8.3-9.6	143.4 - 219.6	3.0 - 5.8
L3	>9.6	>219.6	>5.8

Table 5. Mechanical properties table for pure BC DOE.

DOE Run	Young's Modulus (GPa)	UTS (MPa)	Elongation to Break (%)
1	9.0	224.2	5.0
2	6.4	221.2	6.3
3	8.4	187.0	5.8
4	6.0	149.2	6.5
5	9.6	181.4	3.8
6	10.2	219.6	4.6
7	9.3	130.5	2.5
8	9.8	143.4	2.9
9	9.5	123.0	3.0

Based on the Taguchi matrix, effect of each hot-pressing factor on the mechanical properties can be summarized and visualized by the plots in Figure 16. The plots were normalized, and the value of the plots represented the relative effect of low, medium, and high level of the processing factors. Among all the samples, low processing time (5 min) results in highest Young's Modulus, UTS, while medium pressing time (10min) maximized the EtB. As temperature and pressure increase, the Young's modulus increases, though pressure and temperature maximized Young's modulus and UTS at different levels. Low time (5 min), temperature (120℃) and medium

pressure (10 MPa) were needed to maximize the ultimate tensile strength, while medium time (10 min), low temperature (120°C) and pressure (5 MPa) were required to maximize the EtB.

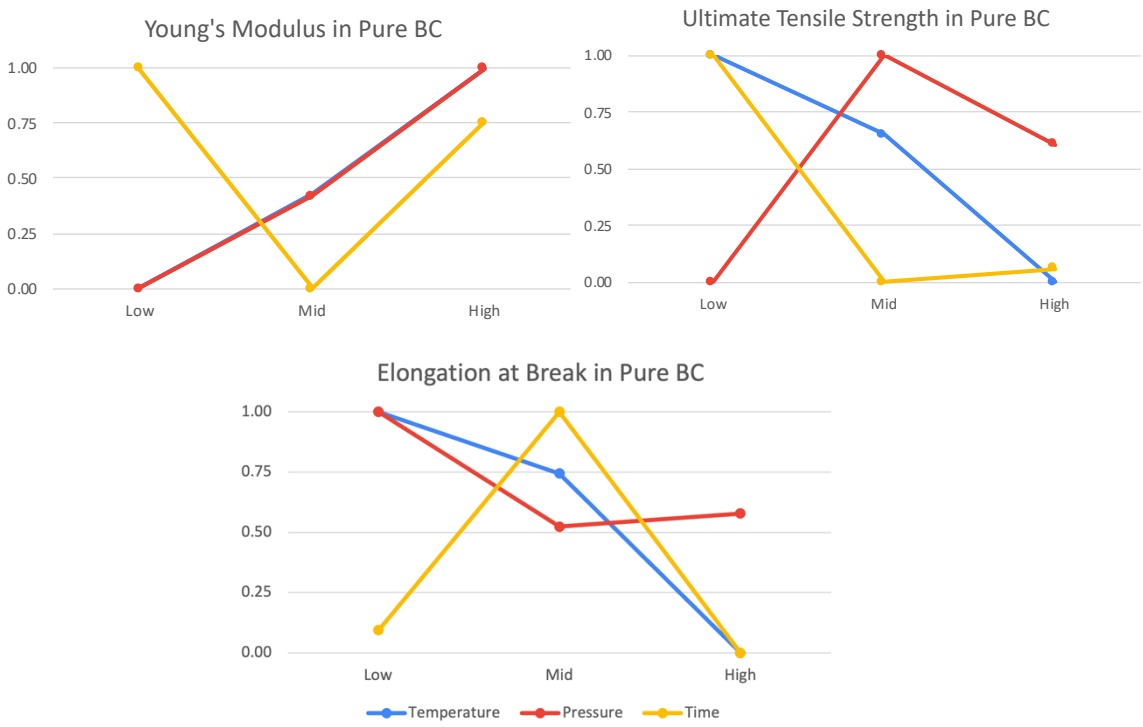

Figure 16. Normalized respective effects of each processing factors in three levels on pure BC, corresponding to each response (Young's modulus, Ultimate tensile strength, and Elongation at break).

The degree of crystallinity was measured in the single-layer pure BC to understand the mechanical difference among samples processed in various conditions (Figure 17). Theoretically, cellulose that has higher crystallinity results in better mechanical properties[3]. However, the differences in crystallinity between our samples, varied insignificantly, ranging from 89% to 91% (Table 6), while there was a significant difference in their mechanical properties as described before. The various levels of mechanical properties could be due to the orientations of crystals or different crystal polymorphs. One possible source for orientation-induced changes is that during

air drying, pure BC pellicles were rolled with a rolling pin multiple times to remove access water, which may have introduced fibril alignment during the rolling process as the pellicle remained in a hydrated state [2]. Such changes in fibril orientation can subsequently alter the mechanical performance of BC. In addition, phase analysis from XRD or small angle x-ray scattering for crystal orientation can be done in the future to test our hypothesis and quantify cellulose polymorph changes.

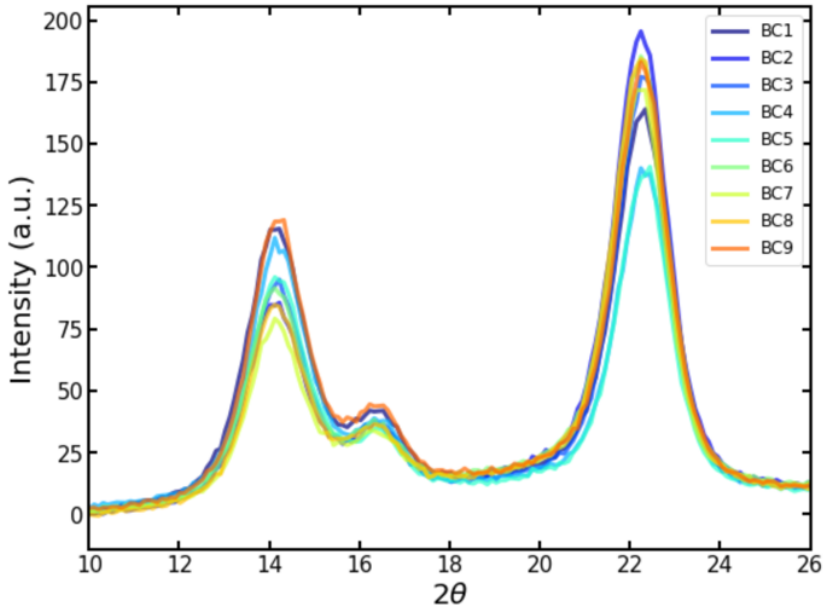

Figure 17. XRD measurement of Pure BC processed with Taguchi matrix (Sample 1-9).

Table 6. Crystallinity and contact angle results from the pure BC samples

DOE Standard Run #	Crystallinity (%)	Contact Angle [°]
1	90.2	56.11
2	91.4	46.58
3	91.2	30.64
4	89.4	35.49
5	89.0	38.01
6	90.7	49.41
7	90.0	42.12
8	90.7	38.56
9	91.0	42.91

Contact angle was measured to study the surface water properties change after hot-pressing. Significant differences of contact angle were seen in Table 6, ranging between 30.6° to 56.1°. The absolute highest contact angle of 56.1° was seen in Sample 1 (120℃, 10 min, and 5 MPa) which were processed in lowest levels in temperature, time, and pressure (Figure 18). In the effect plots, the increase of processing conditions decreased the contact angle (Figure 19). A proposed reason for the contact angle changes is that as processing levels increase, the surface roughness is reduced. Based on the Cassie-Baxter model [42], the increase of surface roughness enables vapor pockets to be trapped underneath the liquid, yielding a higher contact angle. Further testing can be done such as using a profilometer to measure roughness in the future.

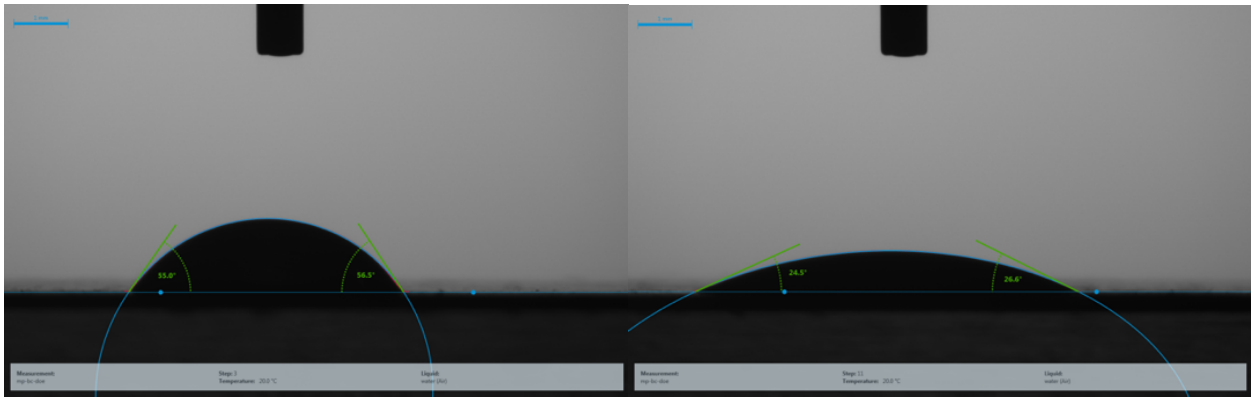

Figure 18. Contact angle image for pure BC DOE RUN1 (left) and RUN3(right).

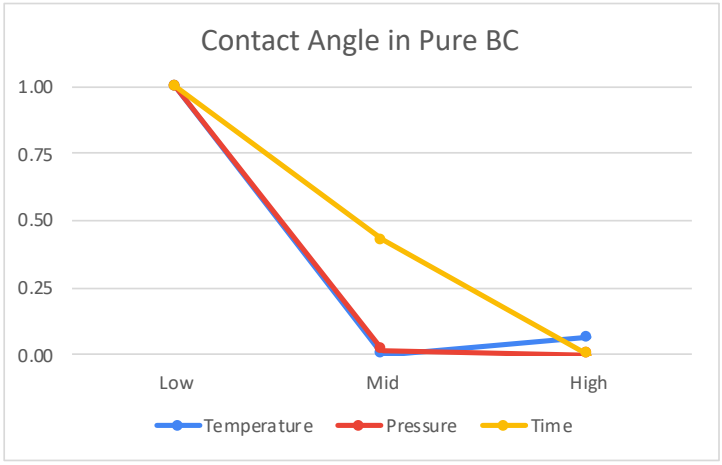

Figure 19. Normalized respective effects of each processing factors in three levels on contact angles of pure BC.

To summarize findings in processing conditions of single-layer pure BC, we found all hot-pressing factors have effect BC mechanical properties. Low time (5 min) maximize Young's modulus and ultimate tensile strength. Young's modulus increased as increasing pressing pressure and temperature, while there was nonlinear trend in the levels of ultimate tensile strength and elongation to break. Though processing time, temperature and pressure had effect on mechanical properties, we did not see significant effect on crystallinity, indicating the change in mechanical properties may result from crystal orientation or polymorphs change. Surface properties were

affected by processing. The less pure BC paper was processed, the less hydrophilic the surface was due to surface roughness. Low temperature, time, and pressure (120℃, 10 min, and 5 MPa) can maximize Young's modulus, ultimate tensile strength, and contact angle.

3.3. Evaluation of different methods to introduce lignin in BC

To prepare the nanocomposites, we were looking for a method that allowed maximum amount of lignin introduction in BC with uniform distribution, and this method need to be compatible with larger samples. We tested three methods to make the BC/lignin nanocomposites: (a) vacuum filtration, (b) ultrasonication, (c) soaking/stirring. As presented in Figure 20, we found all three method allowed uniform lignin introduction in the small samples. However, soaking upon stirring was chosen since it gave better uniformity in larger area sample.

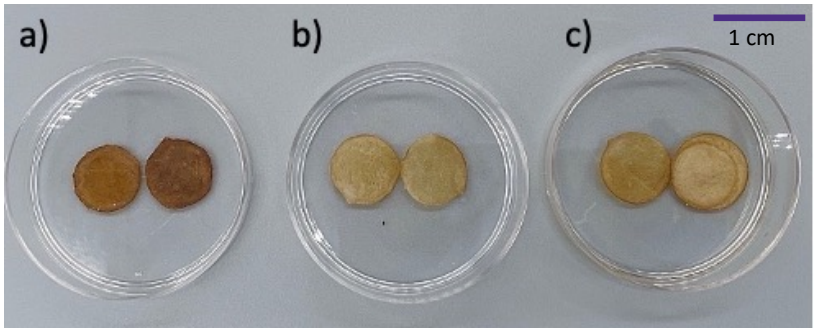

Figure 20. Air-dried BC/lignin nanocomposite with three different methods to introduce lignin. a) Vacuum filtration; b) Ultrasonication; c) Soaking/stirring.

3.4. Optimization of thermomechanical processing conditions to fabricate BC/lignin nanocomposites

After selecting the best method to introduce lignin content into BC, we processed the nanocomposites paper using hot pressing conditions in the same Taguchi matrix as we did for pure

BC with a set lignin concentration. Figure 21 is the hot-pressed samples of BC/lignin nanocomposites.

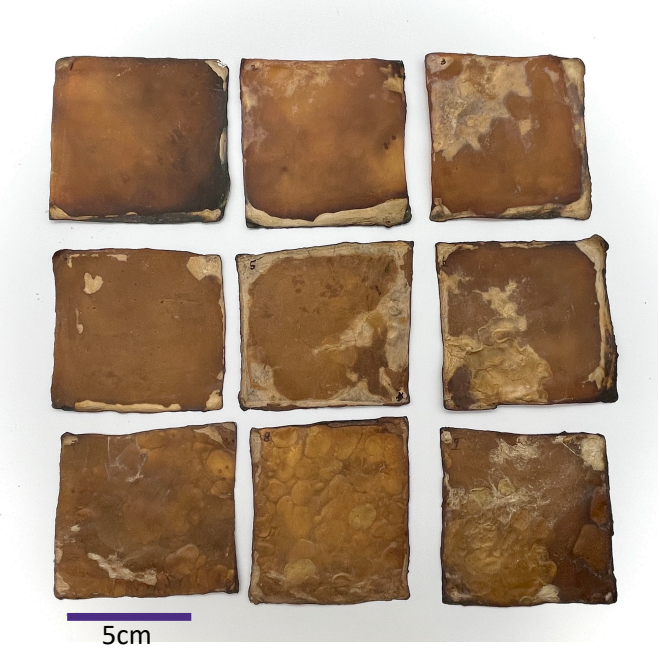

Figure 21. BC/lignin nanocomposites after DOE processing.

From the morphologies of BC/lignin nanocomposites, all samples were infused by lignin. Only sample 1 (120℃, 10 min, and 5 MPa) had completely different morphology, with lignin totally blended in the matrix. In all the rest samples, we saw layers of BC with lignin infiltrated in between fibers, while in some sample such as sample 5 (140℃, 30 min, and 10 MPa) and sample 6 (140℃, 10 min, and 15 MPa), lignin bridged in between layers. (Figure 22)

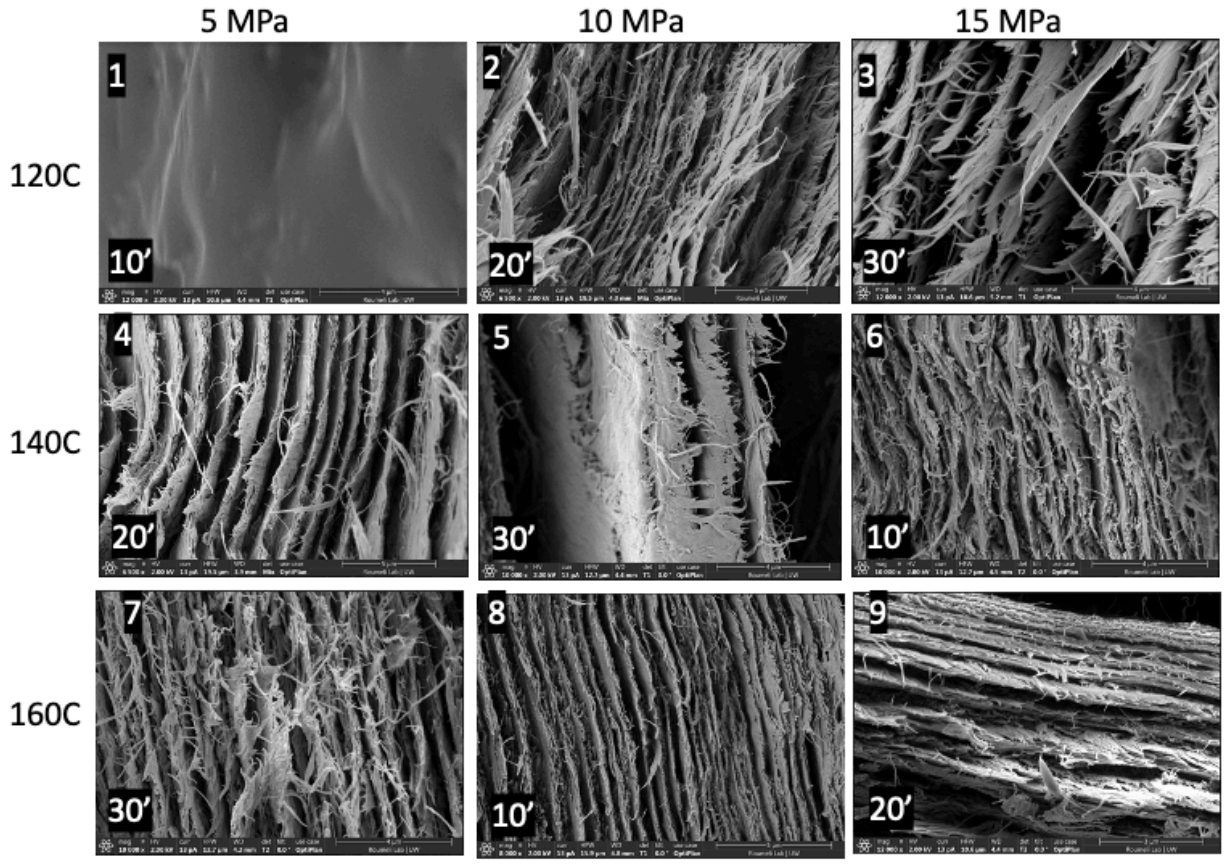

Figure 22. BC/Lignin DOE SEM image, failure of tension at the cross section.

The mechanical properties were shown in Table 8 and Table 9. The highest Young's modulus and UTS were from samples processed with low to medium time, such as sample 2 (120℃, 20 min, and 10 MPa), sample 4 (140℃, 20 min, and 5 MPa), and sample 6 (140℃, 10 min, and 15 MPa). The samples with highest elongation to break were processed at highest temperature, such as sample 7 (160℃, 30 min, and 5 MPa), and sample 8 (160℃, 10 min, and 10 MPa). More specifically, sample 7 had almost double the average of EtB of all the other BC/lignin nanocomposites samples, reaching up as high as 10% elongation, which was also 4 times higher than pure BC processed in the same conditions (about 2.5%).

Table 7. Assignment of mechanical results to three levels based on Quartile 1 and Quartile 3 on BC/lignin nanocomposite.

Level	Young's Modulus (GPa)	UTS (MPa)	Elongation to Break (%)
L1	<5.1	<112.9	<4.6
L2	5.1-6.8	112.9 - 136.2	4.6-5.6
L3	>6.8	>136.2	>5.6

Table 8. Mechanical properties table for BC/lignin nanocomposite DOE.

DOE Run	Young's Modulus (GPa)	UTS (MPa)	Elongation to Break (%)
1	6.4	112.9	4.6
2	8.1	169.6	4.2
3	5.9	128.4	6.2
4	6.8	136.2	5.6
5	5.1	123.5	4.7
6	7.3	160.9	3.9
7	3.3	68.0	10.2
8	2.2	61.9	4.9
9	6.3	133.5	5.0

Figure 23 describes the effects of processing factors on the selected mechanical properties of BC/lignin nanocomposites. As we saw in Pure BC, the lowest time level maximized both Young's modulus and ultimate tensile strength. Here in BC/lignin nanocomposites, time, in medium level (10min) instead of the low level (5min) also maximized Young's modulus simultaneously with UTS. High pressure gave the highest Young's modulus and UTS at the same time. Low and medium temperature gave the highest Young's modulus and UTS respectively. Low pressure and high temperature and time contributed to the maximum of EtB.

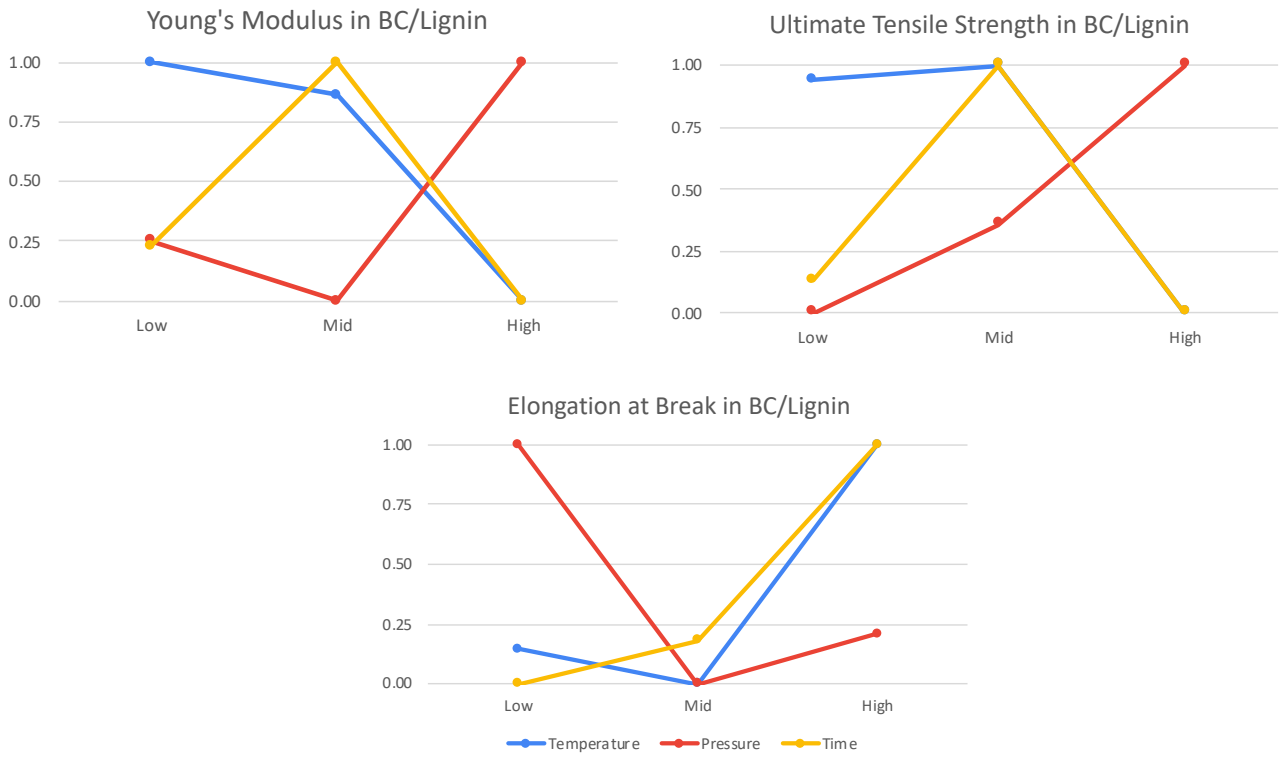

Figure 23. Normalized respective effects of each processing factors in three levels on BC/lignin nanocomposite, corresponding to each response (Young's modulus, Ultimate tensile strength, and Elongation at break).

Crystallinity analysis revealed differences in the BC/lignin nanocomposites (Figure 24 and Table 9). The absolute minimum crystallinity was found in sample 7 (85.8%) that was processed at the highest temperature and time, while other samples had higher crystallinity (88.8±1.5 %), indicating highest pressing time and temperature resulted in most amorphous content. The rest of condition had no significant effect in crystallinity. Therefore, we found that the lower the mechanical properties, the lower crystallinity of the sample and therefore the better distribution of lignin content.

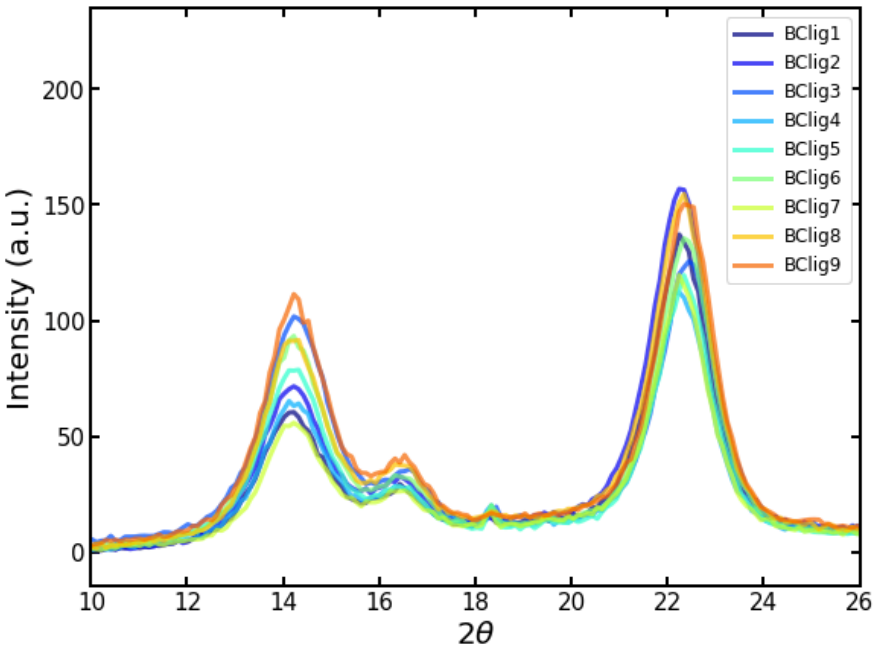

Figure 24. XRD measurement of BC/lignin nanocomposites DOE.

Table 9. Crystallinity and contact angle results from the BC/Lignin nanocomposite samples

DOE Standard Run #	Crystallinity (%)	Contact Angle [°]
1	88.1	31.94
2	89.5	54.83
3	89.3	47.47
4	86.1	51.52
5	87.5	42.57
6	89.2	34.99
7	85.8	55.63
8	90.1	50.98
9	90.8	40.21

In the contact angle study, we found processing affected contact angle in BC/lignin nanocomposites. The absolute maximum contact angle was found in sample 7 with 55.6° while other samples had 44.3±8.3°(Figure 26). Therefore, we found with the higher temperature and

time BC/lignin nanocomposites was processed, the lower mechanical properties, the lower crystallinity, the better lignin distribution which would eventually result in higher contact angle. This was aligned with our initial hypothesis of the study since lignin was amorphous and more hydrophobic than bacterial cellulose. It should be noted that there were different trends in contact angle in response to processing conditions in nanocomposites compared to pure BC. Here the highest processed samples gave the maximum contact angle (Figure 25), while in pure BC it was the lowest, showing lignin impregnation affect the nanocomposite hydrophobicity significantly.

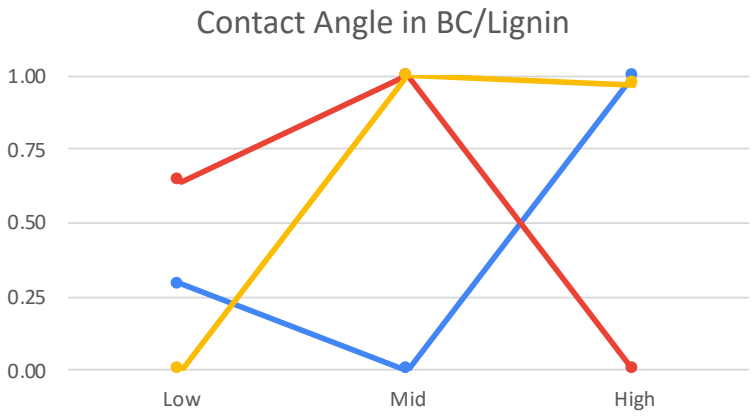

Figure 25. Normalized respective effects of each processing factors in three levels on contact angle of BC/lignin nanocomposite.

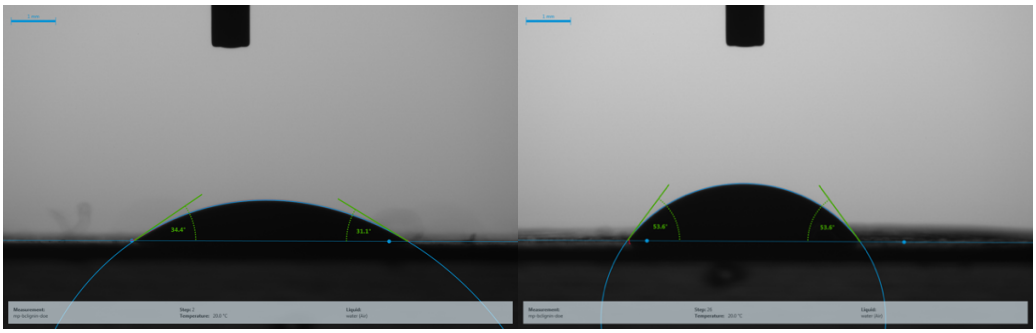

Figure 26. Contact angle image for BC/lignin nanocomposite DOE RUN1 (left) and RUN7(right).

In an effort to test the long-term hydrophobicity performance of our samples, we conduct a new round of contact angle test on the samples with previously determined highest contact angle from both data sets, after 1 month of storage in ambient conditions (room temperature, humidity approximately 40% RH). We monitor the contact angle of sample 1 from the Pure BC and sample 7 from the BC/lignin set with respect to time (Figure 27). The contact angle of BC/lignin nanocomposites which after fabrication was 55.6±5.5°, was now found to be 66.5±6.3° and stabilize around 50±5.5°, at 75 seconds. We notice that the standard deviation in the leveled off values covers the previously measured value of 55.6° so the long-term hydrophobicity of the samples is confirmed and even after storing for 1 month in ambient conditions, the contact angle does not decrease. On the other hand, the contact angle of the pure BC sample 1 was previously measured to be 56.1±11.5°, yet the new tests reveal a much lower contact angle after storage, starting from 42.0±7.5° and decreased further to around 37±3.8°, at 30 seconds. Thus, the long-term storage of the samples was proven to lead to a significant contact angle reduction in the pure BC, while the nanocomposite was found to have the same steady-state response. This can be related to cellulose uptaking water from the environment while being stored, thus becoming more hydrophilic with time, approaching the expected ultra-hydrophilic response that it has naturally. On the other hand, in the composite, lignin is wetting and binding the cellulose fibrils, thus the contact angle is not reversible, and the steady-state properties remain around 50-60^{o} over time. Ultimately results show that the introduction of lignin allows for a long-term improvement in the hydrophobicity of BC, while well hot-pressing leads to only temporary changes in pure BC.

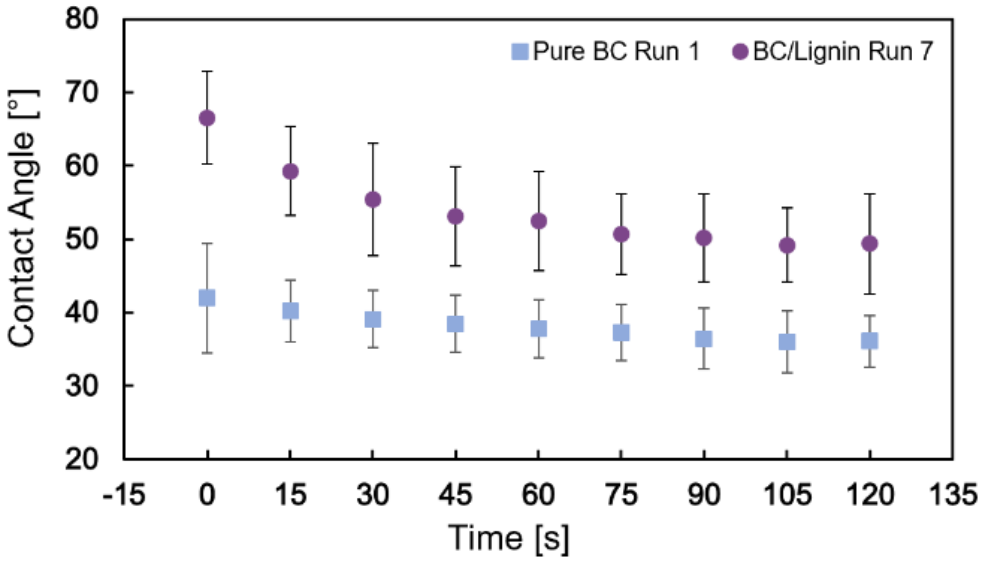

Figure 27. Contact angle change of best performing samples (Pure BC sample 1 and BC/lignin sample 7) with respect to time.

To summarize findings in BC/Lignin nanocomposites, we found there were effects of processing conditions in bulk mechanical properties. Medium time (20min) maximized Young's modulus and UTS, while high pressure gave the highest Young's modulus and UTS. Low pressure and high temperature and time enabled highest EtB. Sample that with lowest crystallinity or more amorphous content had highest extensibility, and lowest Young's modulus and UTS. We found that hydrophobicity of BC can be controlled by either introduction of lignin or processing BC in different pressing conditions. In BC/lignin nanocomposites, the most amorphous sample was also the one with highest EtB and maximum contact angle.

We also found that by introducing lignin into BC and making BC/lignin nanocomposites, the elongation to break was improved, though other mechanical properties such as Young's modulus and ultimate tensile strength were decreased. At certain conditions, lignin introduction add hydrophobicity characteristic to the BC, thus contact angle was improved. The high

temperature and time made the most amorphous nanocomposite, resulting in highest elongation to break and contact angle.

3.4.2. Thermal analysis on BC/lignin nanocomposite

We conducted thermalgravimetric analysis to understand the thermal properties in the BC/lignin nanocomposites. BC/lignin nanocomposites had thermal properties in between pure lignin and pure BC, indicating that there was BC and lignin interaction in the nanocomposites (Figure 28).

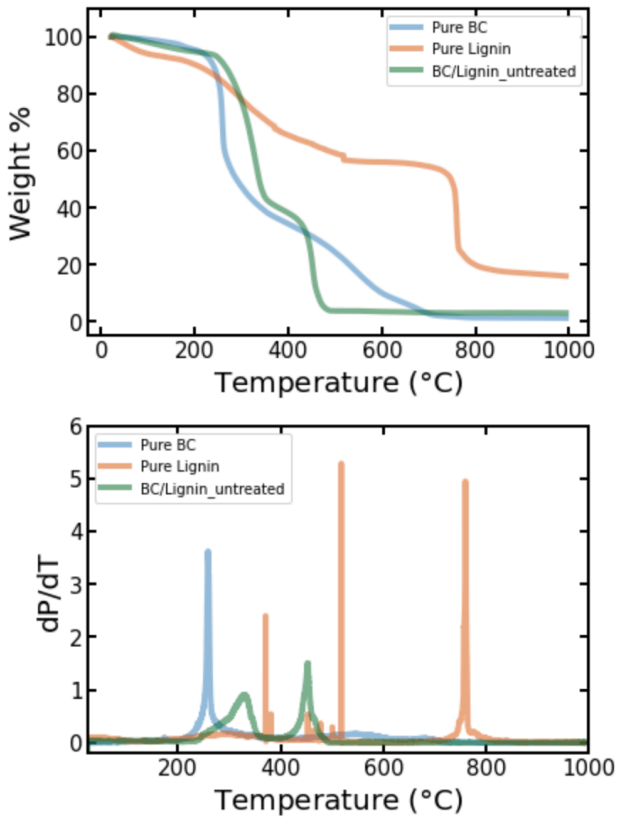

Figure 28. Mass loss curve of thermalgravimetric measurement of pure BC, Pure BC, and BC/lignin without hot pressing conditions.

3.4.3. FTIR analysis on Pure BC and BC/lignin

We also conducted FTIR analysis on pure BC and BC/lignin samples. Table 10 shows the FTIR spectrum peak summary table from literature. In Figure 29, we show an example plots of FTIR spectrum with comparison between pure BC and BC/lignin nanocomposites, confirming the presence of lignin. Future analysis on FTIR can reveal possible interaction between BC and lignin in the nanocomposites.

Table 10. FTIR spectrum summary table from literature for pure BC and BC/lignin nanocomposite. (Lignin characteristic peak was highlighted in the table).

Seen in Pure BC?	Seen in BC/Lignin ?	Wavenumber peaks (cm^{-1})	Peak Assignment	Polymer Source	Reference
Y	Y	3433, 3400, 3328, 3346	-OH stretching of hydrogen bonds	Cellulose I, Lignin	[43], [44], [45], [46], [47], [48], [49]
-	Y	2930	-CH_2 and -CH_3 asymmetric vibration (guaiacyl-syringyl)	Lignin	[48], [49]
Y	Y	2900	-C-H stretching	Cellulose I, Cellulose II, Lignin	[43], [44], [45], [46]
Y	Y	1630	-OH of bending of absorbed water	Cellulose I, Cellulose II	[43], [44], [45], [46]
-	Y	1600	C=O stretching (Conjugated)	Lignin	[47]
-	Y	1593, 1518, 1513	Aromatic skeletal vibrations	Lignin	[47], [50], [51]
-	Y	1506, 1517	C=C aromatic symmetrical stretching	Lignin	[45], [48], [49], [51]
-	Y	1458	C-H asymmetric deformations in	Lignin	[47], [48], [49], [51]

			-CH_2 and -CH_3		
Y	Y	1423	Planar HCH, OCH bending vibration	Cellulose	[45], [46]
-	Y	1397	Phenolic OH and aliphatic C-H in methyl groups	Lignin	[47]
Y	Y	1380,1368, 1362	Planar -CH bending	Cellulose I	[43], [44], [45], [48]
-	Y	1328	Syringyl ring (S-ring) and guaiacyl ring (G-ring)	Lignin	[48], [50], [51]
Y	Y	1317	-CH2 rocking vibration	Cellulose	[45]
-	Y	1268, 1246	C=O and G-ring stretching	Lignin	[45], [47], [48], [49], [50]
-	Y	1234	C=O and S-ring stretching	Lignin	[48], [51]
-	Y	1215-1220	C-C, C-O, C=O stretching	Lignin	[50]
Y	Y	1202	C-O-C symmetric stretching	Cellulose	[45]
Y	Y	1155	C-O-C asymmetric stretching	Cellulose	[44], [46], [48]
-	Y	1151, 1140	CH stretching in G-ring	Lignin	[48], [50]
Y	Y	1048, 1019, 995	C-C, C-OH, C-H ring and side group vibration	Cellulose	[44], [45], [46], [48], [50]
Y	Y	899	COC, CCO, and CCH deformation and stretching	Cellulose I	[43], [44], [45], [46], [48]
-	Y	855, 817	Aromatic C-H out-of-plane deformation in G-ring	Lignin	[48], [50]
-	Y	843	C-H out-of-plane vibration of S-ring	Lignin	[50]
Y	Y	662	C-OH out-of-plane bending	Cellulose	[45], [46]

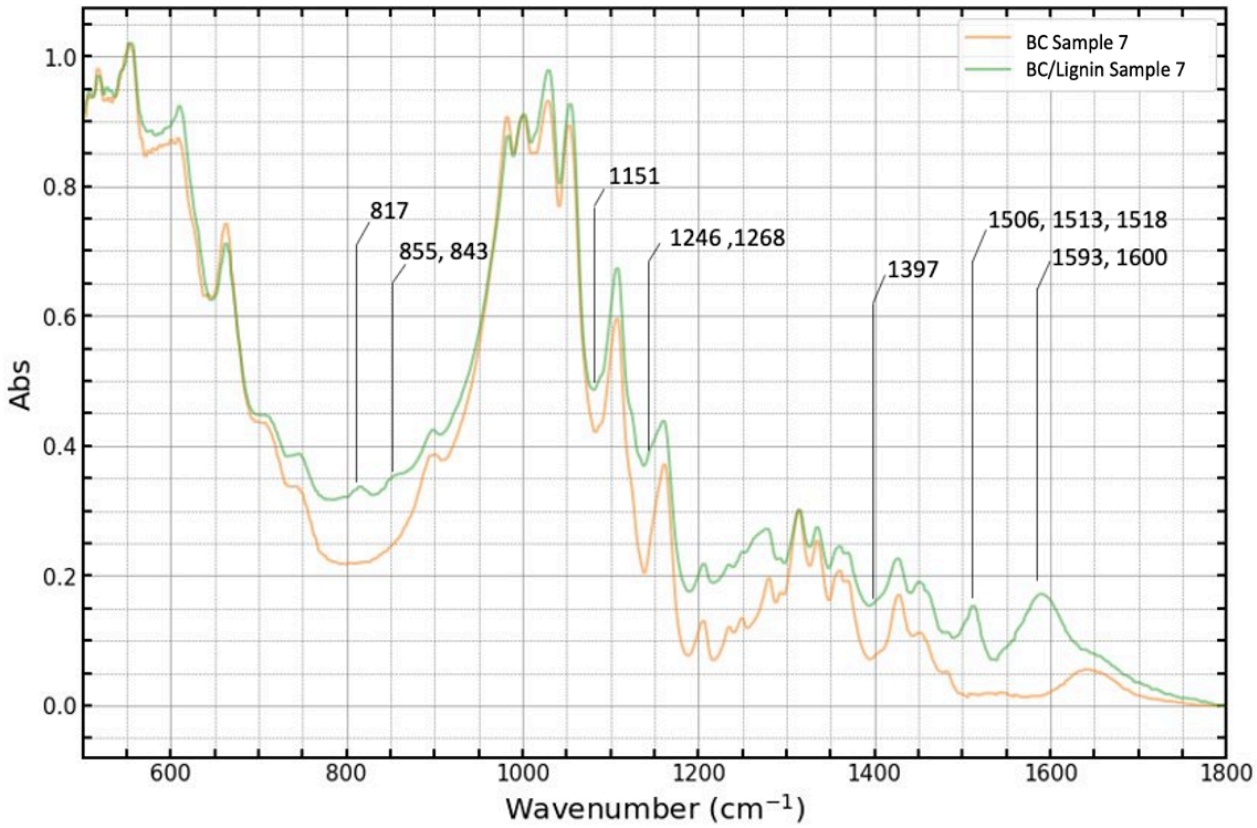

Figure 29. FTIR analysis of Pure BC and BC/lignin nanocomposite processed under 160℃, 5Mpa and 30min.

3.5. Multi-layered nanocomposite

We were also interested in making multi-layered samples to increase the thickness and expand the properties range of BC/lignin nanocomposites (Figure 30). In our hypothesis, lignin not only can improve the water properties but also can act as a binder between each BC layers to strengthen the nanocomposites by load transfer in between the fibril layers. We compared the mechanical properties of 4-layer pure BC and hot-pressed 4-layer BC/lignin nanocomposites (Table 11). As a binder in multi-layered composites, lignin enables 4.3 times improvement Young's modulus, 2.6 times improvement in UTS, though there was no significant difference in

EtB. For water properties, BC/lignin 4-layer contact angle reached up to 53.8° while contact angle of the single-layer BC/lignin nanocomposite processed in the same conditions was 32°.

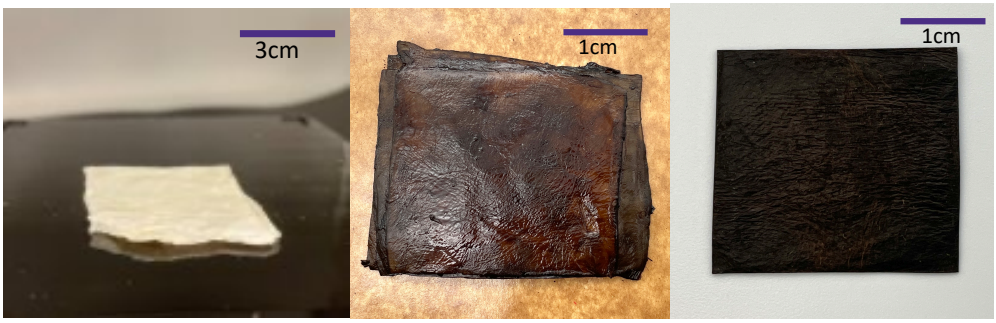

Figure 30. (left) Air dried 4-layer pure BC. (middle) Wet 4-layer BC/lignin. (right) hot-pressed 4-layer BC/lignin with 120C, 5Mpa, 10min.

Table 11. Mechanical properties table for BC/lignin nanocomposite DOE.

Sample	Young's Modulus (GPa)	UTS (MPa)	Elongation to Break (%)
Pure BC 4-layer	1.2	28.1	1.6
BC/lignin 4-layer	5.2	72.8	2.1

4. Conclusions

The goal of this study was to understand examine effects of lignin as a binder to improve the performance of both single-layer and multi-layered bacterial cellulose. We conducted a systematic analysis of the effects of processing conditions such as hot-pressing time, temperature and pressure on the mechanical properties, morphology, crystallinity, and water properties of pure BC and BC/lignin nanocomposites. We firstly focused on the processing conditions effects on pure BC, then compared the findings in BC/lignin nanocomposites. We also studied the effects of lignin acting as a binder in both single-layer and multi-layered nanocomposites.

The introduction of lignin enables altering mechanical and water properties of bacterial cellulose. In multi-layered nanocomposites, lignin as a binder increases Young's modulus and strength. The contact angle in multi-layered nanocomposites is also increased comparing to the same processing conditions of single-layer nanocomposites and remains the same over time. In single-layer, the introduction of lignin improves elongation to break, at the expense of Young's modulus and strength.

In terms of the processing conditions, we found that processing conditions affect mechanical properties differently in the single-layer BC and BC/lignin composites. In pure BC, low time, pressure, and temperature maximize Young’s modulus and strength, while in BC/lignin nanocomposites, medium time and pressure contribute to high Young’s modulus. We found two ways to alter contact angle, by different hot-pressing conditions on pure BC, that can temporarily improve the hydrophobicity, but this effect is transient and is reversed over storing the samples over time, while introducing lignin to the BC matrix leads to long-term stable hydrophobicity effects. In pure BC, less processing leads to rougher and less hydrophilic surface, while in

BC/lignin nanocomposite, more processing gives rise to better lignin distribution and better water surface properties.

5. Future work

It is apparent that processing of BC/lignin nanocomposites affects the mechanical properties differently. In some cases, either setting the temperature or pressure at medium level can maximize the response. A Life Cycle Assessments (LCA) can be conducted to select most effective processing conditions based on the energy and cost of each processing conditions.

Due to limitations of time, only one lignin concentration was studied in this work, so more study can be done on various lignin concentration. Even though we knew the concentration of the lignin solution, the Klason lignin test can be done to confirm the actual lignin content within the dried BC/lignin nanocomposites.

In pure BC, we measured significant effects of the processing conditions on the mechanical properties of the obtained films, while we found no significant difference in crystallinity. A fiber orientation study as well as a phase analysis can be done to understand how rolling motion can align the crystal in BC and therefore change the mechanical properties.

6. References

1. Shanmugam, V. *et al.* Polymer Recycling in Additive Manufacturing: an Opportunity for the Circular Economy. *Mater. Circ. Econ.* **2**, 11 (2020).
2. Wang, S. *et al.* Super-Strong, Super-Stiff Macrofibers with Aligned, Long Bacterial Cellulose Nanofibers. *Adv. Mater.* **29**, 1702498 (2017).
3. Moon, R. J., Martini, A., Nairn, J., Simonsen, J. & Youngblood, J. Cellulose nanomaterials review: structure, properties and nanocomposites. *Chem Soc Rev* **40**, 3941–3994 (2011).
4. Zhu, H. *et al.* Anomalous scaling law of strength and toughness of cellulose nanopaper. *Proc. Natl. Acad. Sci.* **112**, 8971–8976 (2015).
5. Ling, S. *et al.* Biopolymer nanofibrils: Structure, modeling, preparation, and applications. *Prog. Polym. Sci.* **85**, 1–56 (2018).
6. Jiang, B. *et al.* Lignin as a Wood-Inspired Binder Enabled Strong, Water Stable, and Biodegradable Paper for Plastic Replacement. *Adv. Funct. Mater.* **30**, 1906307 (2020).
7. Shrivastava, A. Introduction to Plastics Engineering. in *Introduction to Plastics Engineering* 1–16 (Elsevier, 2018). doi:10.1016/B978-0-323-39500-7.00001-0.
8. For the first time: Growth rate for bio-based polymers with 8 % CAGR far above overall polymer market growth. *Renewable Carbon News* (2020).
9. Geyer, R., Jambeck, J. R. & Law, K. L. Production, use, and fate of all plastics ever made. *Sci. Adv.* **3**, e1700782 (2017).
10. The lifecycle of plastics. *World Wildlife Fund (WWF) Australia* (2021).
11. Koncar, V. Composites and hybrid structures. in *Smart Textiles for In Situ Monitoring of Composites* 153–215 (Elsevier, 2019). doi:10.1016/B978-0-08-102308-2.00002-4.

12. Wang, Z., Ganewatta, M. S. & Tang, C. Sustainable polymers from biomass: Bridging chemistry with materials and processing. *Prog. Polym. Sci.* **101**, 101197 (2020).
13. Roumeli, E., Fredricks, J., Jimenez, A. & Law, E. Hierarchical biopolymer-based materials and biological-matrix composites. *Prep* (2021).
14. Jayabalan, R., Malbaša, R. V., Lončar, E. S., Vitas, J. S. & Sathishkumar, M. A Review on Kombucha Tea-Microbiology, Composition, Fermentation, Beneficial Effects, Toxicity, and Tea Fungus: A review on kombucha…. *Compr. Rev. Food Sci. Food Saf.* **13**, 538–550 (2014).
15. Gatenholm, P. & Klemm, D. Bacterial Nanocellulose as a Renewable Material for Biomedical Applications. *MRS Bull.* **35**, 208–213 (2010).
16. Jonas, R. & Farah, L. F. Production and application of microbial cellulose. *Polym. Degrad. Stab.* **59**, 101–106 (1998).
17. Watanabe, K., Tabuchi, M., Morinaga, Y. & Yoshinaga, F. Structural features and properties of bacterial cellulose produced in agitated culture. *Cellulose* **5**, 187–200 (1998).
18. Yamanaka, S. *et al.* The structure and mechanical properties of sheets prepared from bacterial cellulose. *J. Mater. Sci.* **24**, 3141–3145 (1989).
19. Nakagaito, A. N., Iwamoto, S. & Yano, H. Bacterial cellulose: the ultimate nano-scalar cellulose morphology for the production of high-strength composites. *Appl. Phys. A* **80**, 93–97 (2005).
20. Gea, S., Bilotti, E., Reynolds, C. T., Soykeabkeaw, N. & Peijs, T. Bacterial cellulose–poly(vinyl alcohol) nanocomposites prepared by an in-situ process. *Mater. Lett.* **64**, 901–904 (2010).

21. Fink, H.-P. *et al.* Evaluation of new organosolv dissolving pulps. Part II: Structure and NMMO processability of the pulps. *Cellulose* **11**, 85–98 (2004).
22. Takai, M., Tsuta, Y., Hayashi, J. & Watanabe, S. Biosynthesis of Cellulose by Acetobacter Xylinum. III. X-Ray Studies of Preferential Orientation of the Crystallites in a Bacterial Cellulose Membrane. *Polym. J.* **7**, 157–164 (1975).
23. Astley, O. M., Chanliaud, E., Donald, A. M. & Gidley, M. J. Tensile deformation of bacterial cellulose composites. *Int. J. Biol. Macromol.* **32**, 28–35 (2003).
24. Laavanya, D., Shirkole, S. & Balasubramanian, P. Current challenges, applications and future perspectives of SCOBY cellulose of Kombucha fermentation. *J. Clean. Prod.* **295**, 126454 (2021).
25. Martínez Leal, J., Valenzuela Suárez, L., Jayabalan, R., Huerta Oros, J. & Escalante-Aburto, A. A review on health benefits of kombucha nutritional compounds and metabolites. *CyTA - J. Food* **16**, 390–399 (2018).
26. Chen, C. & Liu, B. Y. Changes in major components of tea fungus metabolites during prolonged fermentation. *J. Appl. Microbiol.* **89**, 834–839 (2000).
27. Ross, P., Mayer, R. & Benziman, M. Cellulose biosynthesis and function in bacteria. *Microbiol. Mol. Biol. Rev.* **55**, 35–58 (1991).
28. May, A. *et al.* Kombucha: a novel model system for cooperation and conflict in a complex multi-species microbial ecosystem. *PeerJ* **7**, e7565 (2019).
29. Reiss, J. Influence of different sugars on the metabolism of the tea fungus. *Z. F□r Lebensm.-Unters. -Forsch.* **198**, 258–261 (1994).

30. Jayabalan, R. *et al.* Preservation of Kombucha Tea—Effect of Temperature on Tea Components and Free Radical Scavenging Properties. *J. Agric. Food Chem.* **56**, 9064–9071 (2008).
31. Mukadam, T. A., Punjabi, K., Deshpande, S. D., Vaidya, S. P. & Chowdhary, A. S. Isolation and Characterization of Bacteria and Yeast from Kombucha Tea. *Int. J. Curr. Microbiol. Appl. Sci.* **5**, 32–41 (2016).
32. Teoh, A. L., Heard, G. & Cox, J. Yeast ecology of Kombucha fermentation. *Int. J. Food Microbiol.* **95**, 119–126 (2004).
33. De Roos, J. & De Vuyst, L. Acetic acid bacteria in fermented foods and beverages. *Curr. Opin. Biotechnol.* **49**, 115–119 (2018).
34. Shah, N., Ul-Islam, M., Khattak, W. A. & Park, J. K. Overview of bacterial cellulose composites: A multipurpose advanced material. *Carbohydr. Polym.* **98**, 1585–1598 (2013).
35. Yano, S., Maeda, H., Nakajima, M., Hagiwara, T. & Sawaguchi, T. Preparation and mechanical properties of bacterial cellulose nanocomposites loaded with silica nanoparticles. *Cellulose* **15**, 111–120 (2008).
36. Maryam *et al.* Provision of micro-nano bacterial cellulose as bio plastic filler by sonication method. *IOP Conf. Ser. Mater. Sci. Eng.* **223**, 012040 (2017).
37. Zhou, X., Broadbelt, L. J. & Vinu, R. Mechanistic Understanding of Thermochemical Conversion of Polymers and Lignocellulosic Biomass. in *Advances in Chemical Engineering* vol. 49 95–198 (Elsevier, 2016).
38. Karunarathna, M. S. & Smith, R. C. Valorization of Lignin as a Sustainable Component of Structural Materials and Composites: Advances from 2011 to 2019. *Sustainability* **12**, 734 (2020).

39. Yeap, R. Y. The Potential of Lignin to Increase the Hydrophobicity of Micro/nanofibrillated Cellulose (MNFC). (THE UNIVERSITY OF BRITISH COLUMBIA, 2020).
40. Nam, S., French, A. D., Condon, B. D. & Concha, M. Segal crystallinity index revisited by the simulation of X-ray diffraction patterns of cotton cellulose Iβ and cellulose II. *Carbohydr. Polym.* **135**, 1–9 (2016).
41. Sun, W., Tajvidi, M., Hunt, C. G., McIntyre, G. & Gardner, D. J. Fully bio-based hybrid composites made of wood, fungal mycelium and cellulose nanofibrils. *Sci. Rep.* **9**, 1–12 (2019).
42. Sigmund, W. M. & Hsu, S.-H. Cassie–Baxter Model. in *Encyclopedia of Membranes* (eds. Drioli, E. & Giorno, L.) 310–311 (Springer Berlin Heidelberg, 2016). doi:10.1007/978-3-662-44324-8_1381.
43. Suryanto, H., Aminnudin, Mahsuli, Wijaya, H. W. & Yanuhar, U. FTIR analysis of alkali treatment on bacterial cellulose films obtained from pineapple peel juice. *IOP Conf. Ser. Mater. Sci. Eng.* **1034**, 012145 (2021).
44. Autal, R., Adamus, G., Kwiecien, M., Radecka, I. & Hooley, P. Production and characterization of bacterial cellulose before and after enzymatic hydrolysis. *Afr. J. Biotechnol.* **16**, 470–482 (2017).
45. Dai, D. & Fan, M. Characteristic and Performance of Elementary Hemp Fibre. *Mater. Sci. Appl.* **01**, 336–342 (2010).
46. Jia, Y. *et al.* Preparation and characterization of a novel bacterial cellulose/chitosan bio-hydrogel. *Nanomater. Nanotechnol.* **7**, 184798041770717 (2017).
47. Rashid, T., Kait, C. F. & Murugesan, T. A "Fourier Transformed Infrared" Compound Study of Lignin Recovered from a Formic Acid Process. *Procedia Eng.* **148**, 1312–1319 (2016).

48. Reyes-Rivera, J. & Terrazas, T. Lignin Analysis by HPLC and FTIR. in *Xylem* (eds. de Lucas, M. & Etchhells, J. P.) vol. 1544 193–211 (Springer New York, 2017).
49. Nikafshar, S. *et al.* Catalyzed Synthesis and Characterization of a Novel Lignin-Based Curing Agent for the Curing of High-Performance Epoxy Resin. *Polymers* **9**, 266 (2017).
50. Boeriu, C. G., Bravo, D., Gosselink, R. J. A. & van Dam, J. E. G. Characterisation of structure-dependent functional properties of lignin with infrared spectroscopy. *Ind. Crops Prod.* **20**, 205–218 (2004).
51. Zhou, G., Taylor, G. & Polle, A. FTIR-ATR-based prediction and modelling of lignin and energy contents reveals independent intra-specific variation of these traits in bioenergy poplars. *Plant Methods* **7**, 9 (2011).